Journal Pre-proofs

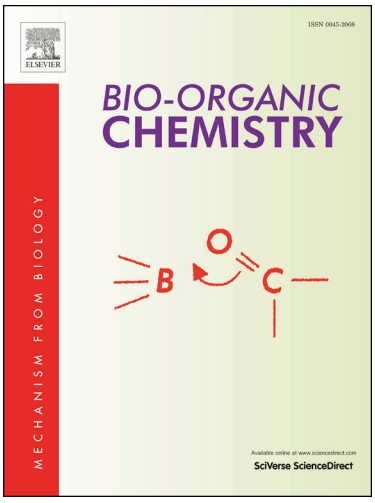

Potent Arylamide Derivatives as Dual-Target Antifungal Agents: Design, Synthesis, Biological evaluation, and Molecular Docking Studies

Yue Dong, Xinyong Liu, Yunfei An, Min Liu, Jun Han, Bin Sun

PII: S0045-2068(20)30119-X
DOI: https://doi.org/10.1016/j.bioorg.2020.103749
Reference: YBIOO 103749

To appear in: *Bioorganic Chemistry*

Received Date: 15 January 2020
Revised Date: 1 February 2020
Accepted Date: 9 March 2020

Please cite this article as: Y. Dong, X. Liu, Y. An, M. Liu, J. Han, B. Sun, Potent Arylamide Derivatives as Dual-Target Antifungal Agents: Design, Synthesis, Biological evaluation, and Molecular Docking Studies, *Bioorganic Chemistry* (2020), doi: https://doi.org/10.1016/j.bioorg.2020.103749

Potent Arylamide Derivatives as Dual-Target Antifungal Agents: Design, Synthesis, Biological evaluation, and Molecular Docking Studies

Yue Dong [a,1], Xinyong Liu [b,1], Yunfei An[a], Min Liu [a], Jun Han [a], Bin Sun, [*, a, b]

[a]*Institute of BioPharmaceutical Research, Liaocheng University, 1 Hunan Road, Liaocheng 252000, PR China*

[b]*Department of Medicinal Chemistry, School of Pharmaceutical Sciences, Shandong University, 44 West Culture Road, Jinan 250012, PR China.*

ABSTRACT

Fungal infections have become a serious medical problem due to the high infection rate and the frequent emergence of drug resistance. Ergosterol is an important structural component of the fungal cell membrane, its synthetases (squalene epoxidase (SE) and 14α-demethylase (CYP51)) are considered as the key points to block the ergosterol synthesis. In this study, we designed a series of dual-target arylamides derivatives based on the analysis of active sites (SE, CYP51). Subsequently, these target compounds were synthesized, and their antifungal activity was evaluated. Most of compounds demonstrate the potent antifungal activity against multiple *Candida spp*. and *A. fum*. In particular, the antifungal activities of compounds **10b** and **11c** are not only superior to positive control drugs, but also have significant inhibitory effects on drug-resistant fungi (*C.alb. Strain100*, *C.alb. Strain103*). Therefore, their action mechanism was further studied. Cellular uptake and electron microscopy observation showed that target compounds were able to enter fungal cytoplasmic region through free diffusion, and destroyed cell membrane structure. At the same time, preliminary mechanisms have demonstrated that they can affect the synthesis of ergosterol by inhibiting the activity of dual targets. It is worth noting that they also can exhibit excellent antifungal activity and low toxic side effects *in vivo*. Their ADMET properties and binding models were established will be useful for further lead optimization.

Key Words: Fungal infections, Dual-target inhibitors, SE, CYP51, Antifungal activity

1. Introduction

In the past two decades, the incidence of invasive fungal in fections (IFIs) has

markedly increased with environmental degradation and drug abuse [1,2], especially for some immunocompromised patients, such as organ transplant recipients, cancer patients, and those infected with AIDS [3]. The recent analyses of hospital data revealed that the annual growth rate of invasive fungal infections increased by 16%, and the annual mortality rate of invasive fungal infections increased by 33% [4,5]. The most common culprits for fungal infections arise from the *Candida spp.*, *Cryptococcus neoformans,* and *Aspergillus spp*. Among them, *Candida albicans* infection accounted for 78.9% [6]. Fungal infectious diseases have begun to seriously threaten human health.

The clinically available antifungal agents can be divided into two categories including the antibiotics (e.g., amphotericin B, caspofungin, and nystatin) and small molecule compounds (e.g., naftifine, fluconazole, and voriconazole) [7,8]. Although these antibiotic fungal inhibitors show the excellent clinical characteristics, they also have obvious defects such as inability to attain oral administration, difficulty in synthesis and high price [9]. At present, allylamine (SE inhibitors; e.g., naftifine, terbinafine, and tolnaftate) and azoles (CYP51 inhibitors; e.g., fluconazole, voriconazole, and itraconazole) antifungal drugs as small molecule compounds have been selected as the most widely first-line antifungal drugs [10,11]. They can inhibit separately the key squalene epoxidase (SE) and 14α-demethylase (CYP51) activity, and block the ergosterol synthesis [12,13]. Some upstream components and toxic intermediates (e.g., lanosterol and 14a-methyl-3-6-diol) are continuously accumulated in cells, which can causes changes in cell membranes and exudation of contents, and eventually lead to fungal death [14-16]. However, these antifungal agents are also challenged by drug resistance, narrow antifungal spectrum, low bioavailability, or other drawbacks, including nephrotoxicity and hepatotoxicity [17,18]. Dual-target drugs or multi-target drugs can synergistically inhibit the activity of double or multiple-target enzymes, and reduce the probability of side effects, especially the emergence of fungal resistance [20-21]. Based on this principle, we plan to construct the novel dual-target antifungal inhibitors by analyzing the active sites of dual-target (SE, CYP51).

In the study, the method of fragment-based drug discovery (FBDD) was applied to design a series of novel dual-target (SE, CYP51) antifungal inhibitors. Subsequently, these compounds were synthesized, and the antifungal activity *in vivo* and *in vitro* were evaluated. At the same time, the preliminary action mechanism was also explored and proved using cell-based and biochemical assays. This study will provide a new direction to design the novel antifungal compound.

2. Results and discussion

2.1. The Design of Combinative Dual-Target Antifungal Agents

A new type of merged dual-target compounds can be obtained by analyzing the active sites and the common pharmacophore features (SE, CYP51) [22-24]. In the study, naftifine (SE inhibitor) and fluconazole (CYP51 inhibitor) were selected as research object, and they were docked into the target enzyme (SE, CYP51) at the same time, molecular binding patterns show similar conformations. In the active cavity of the SE, they can form the hydrophobic interaction with key amino acid residues (Asp 39, Met 306, Asp 329 and Pro336). In the active cavity of the CYP51, their core groups can form the hydrophobic interaction with the key amino acid residues (Leu129, Ile 139,

Tyr 140 and Leu 380). It was worth noting that the azole group of fluconazole can form the important coordination bond with heme in the bottom region of active site, which greatly enhances the binding ability of fluconazole (**Figure. 1A**). In addition, their pharmacophore features also show a certain similarity in spatial distribution [8]. The hydrophobic groups of naftifine and fluconazole can match to the regions of hydrophobic features, and the hydrogen-bond acceptor was positioned in the azole group of fluconazole.

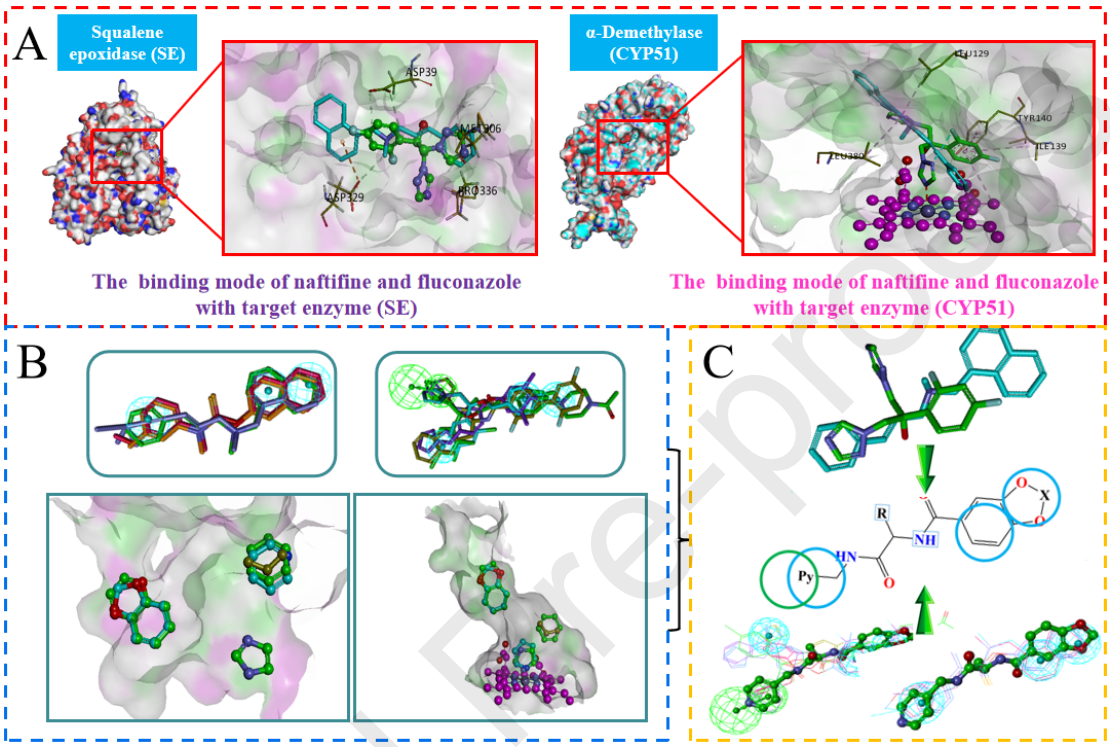

Figure 1. (A) The binding mode of ligand molecules (naftifine, fluconazole) with target enzymes (SE, CYP51); **(B)** The combination pattern of active groups in the active sites (SE, CYP51); **(C)** Design of the novel dual-target antifungal compounds.

Based on the detailed inhibitor-enzyme interaction models, dual-target antifungal agents with new scaffolds were designed using FBDD approach, which was expected to have improved selectivity and specificity. The strategy was to replace the core groups of naftifine and fluconazole in the corresponding active cavities (**Figure. 1B**). The benzo[*d*][1,3]dioxole-5-carboxamide group and 2,3-dihydrobenzo[*b*][1,4] dioxine -6-carboxamide group were selected and substituted the naphthyl group of naftifine and phenyl group of fluconazole. The necessary nitrogen-containing group (pyridine or imidazole) was selected, so that they also can possess the binding ability to form coordination bonds in the active site of CYP51 [25, 26]. Moreover, the different substituted groups in the region (R) were selected to investigate the effect of steric hindrance. Finally, the novel arylamide compounds were constructed by connecting the core groups for subsequent studies (**Figure. 1C**).

2.2. Chemistry

The amidopyridine-containing target compounds **8a-e**, **9a-e**, **10a-e**, **11a-e**, and **12-15** were synthesized according to the route outlined in **Scheme 1** and **Scheme 2** [27, 28]. First, the intermediate benzo[*d*] [1,3] dioxole-5-carbaldehyde (**2a**) and 2,3-

dihydrobenzo[*b*] [1,4] dioxine-6-carbaldehyde (**2b**) were obtained by cyclization reaction. In the process, the commercially available 3,4-dihydroxybenzaldehyde (**1**) was selected as starting material, and it was treated with dibromomethane and dibromoethane to provide these corresponding aldehyde compounds (**2a-b**) in the alkaline conditions. Subsequently, they were further oxidized to obtain the key intermediates benzo[*d*][1,3]dioxole-5-carboxylic acid (**3a**) and 2,3-dihydrobenzo [*b*][1,4] dioxine- 6-carboxylic acid (**3b**) with $KMnO_4$, respectively. On the other hand, L-Glycine, L-Alanine, L-Valine, L-Phenylglycine (**4a-d**) and carbamic acid (**4-1**) were treated with anhydrous ethanol in the presence of $SOCl_2$ to afford the corresponding amino acid esters hydrochloride (**5a-d**, **5-1**). Next, the key intermediates benzo[*d*]1,3 dioxole-5-carboxylic acid (**3a)** and 2,3-dihydrobenzo[*b*] [1,4]dioxine-6-carboxylic acid (**3b**) were converted to the corresponding products (**6a-d, 6-1**) through amidation reaction. Among them, the amide bond of the intermediate **6a** can also be introduced into methyl group (**6a-1**) through methylation reaction. Subsequently, their ester fragments in the presence of 2N sodium hydroxide or lithium hydroxide solution were hydrolyzed to obtain the different organic acids (**7a-e**, **7-1**). Finally, the introduction of pyridyl group, using the corresponding organic acids and aminomethylpyridine via amidation reaction, gave the final target compounds (**8a-e**, **9a-e**, **10a-e**, **11a-e**, and **12-15)** following described.

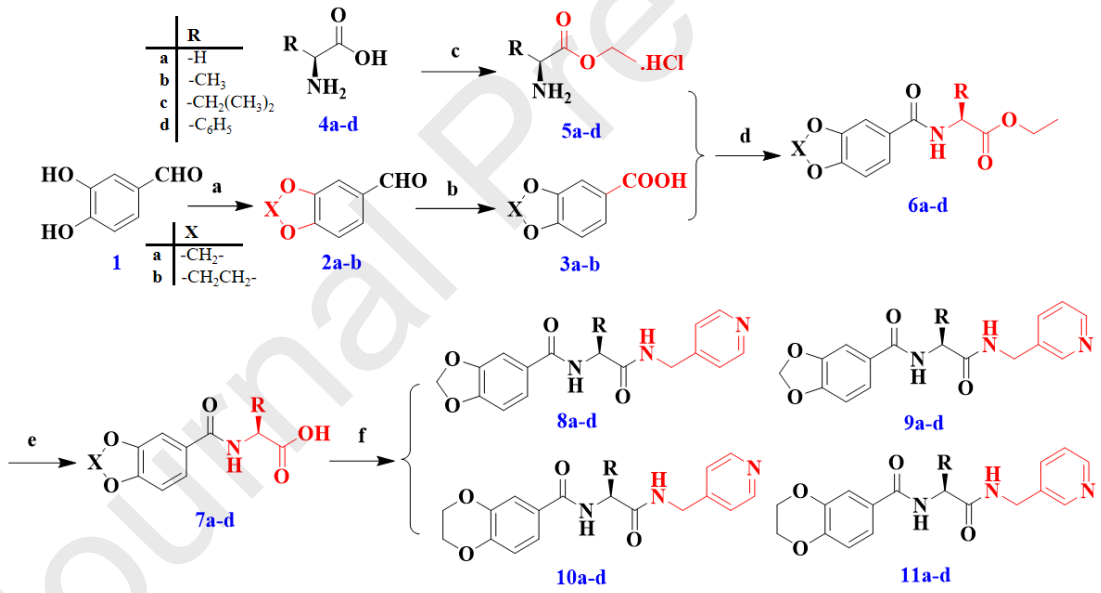

Scheme 1. Reagents and conditions: (a) K_2CO_3, CH_2Br_2 or $BrCH_2CH_2Br$, CuO, reflux, 0.5 h; (b) $KMnO_4$, 80°C, 3 h; (c) $SOCl_2$, CH_3CH_2OH, 5 h; (d) HATU, DIEA, 80°C,7 h; (e) 2N NaOH solution, MeOH, 60°C, 5 h; (f) PyBOP, DIEA, rt, 7 h.

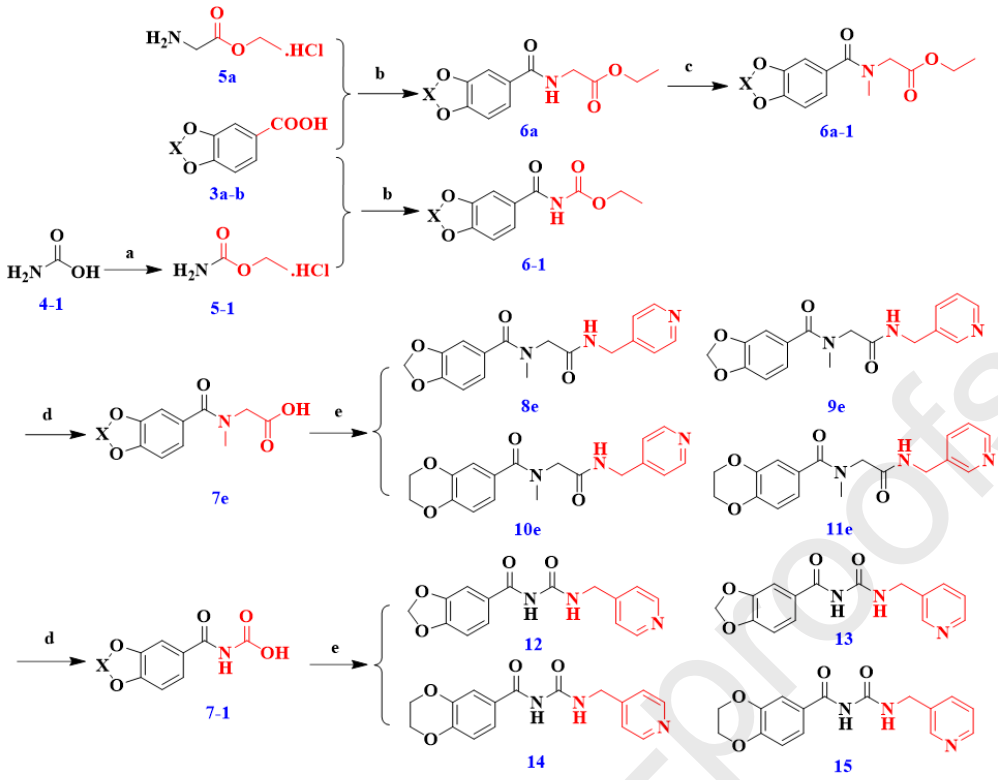

Scheme 2. Reagents and conditions: (a) $SOCl_2$, CH_3CH_2OH, 3 h; (b) HATU, DIEA, 80°C,7 h; (c) CH_3I, K_2CO_3, 25°C,7 h; (d) NaOH solution, MeOH, 60°C, 5 h; (e) PyBOP, DIEA, rt, 7 h.

Amidoimidazole-containing target compounds **(16**, **17**, **19**, and **20)** were prepared according to the synthetic route outlined in **Scheme 3** [29]. Serine (**4-2**) was selected as the junction center, it can react with ethanol to obtain serine ethyl ester hydrochloride (**5-2**). Then, the serine ester was further reacted with the key intermediate (**3a-b**) in the presence of condensation agent to give the required intermediate compounds (**6-2**). Next, they were introduced the imidazole groups to obtain compounds (**16**, **17**) using CDI/imidazole. In addition, some products were further hydrolyzed to obtain the corresponding carboxyl compounds (**18-1**, **18-2**). Finally, the target compounds (**19**, **20**) were synthesized from organic acid and benzylamine via amidation reaction.

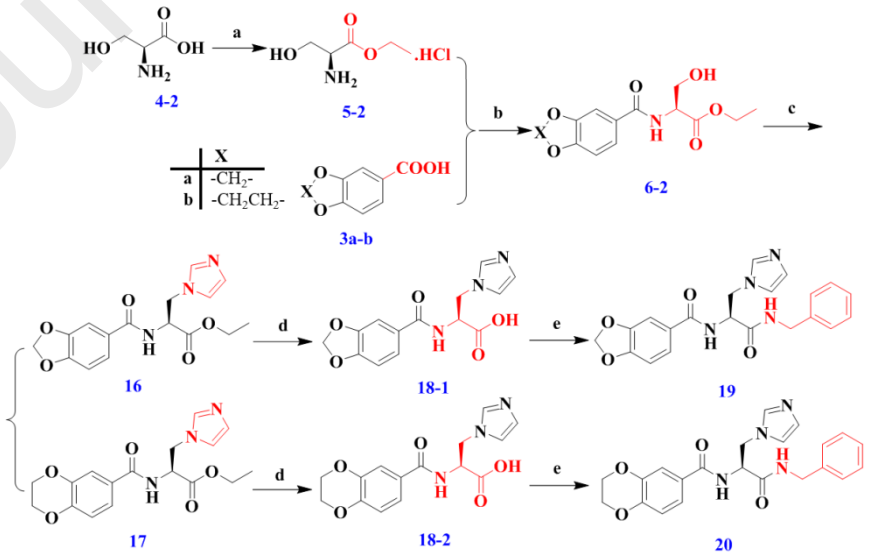

Scheme 3. Reagents and conditions: (a) $SOCl_2$, CH_3CH_2OH, 0.5 h; (b) HATU, DIEA, 80°C,7 h; (c) CDI, Imidazole, 75°C, 7h; (d) 2N NaOH solution, MeOH, 60°C, 5 h; (e) PyBOP, DIEA, rt, 7 h.

2.3. In Vitro Antifungal Activity of Target Compounds

In the study, target compounds **8a-e**, **9a-e**, **10a-e**, **11a-e**, **12-15**, **16**, **17**, **19**, and **20** were evaluated for *in vitro* antifungal activity according the protocols from the NCCLS, the tested strain contains four pathogenic *Candida* and one *Aspergillus fumigatus (A. fum)* [30]. Fluconazole (*FLC*) and naftifine were selected as reference drugs.

Table 1. *In vitro* antifungal activities of the target compounds (MIC, μg/mL).

Compd	R	Nitrogen-containing groups	MIC, μg/mL				
			C.alb.	***C.gla.***	***C.kru.***	***C.tro.***	***A.fum***
8a	H	4-picolinylamine	0.25	2.0	0.5	1.0	8.0
8b	Methyl	4-picolinylamine	1.0	0.5	1.0	0.25	4.0
8c	Isopropyl	4-picolinylamine	1.0	0.25	1.0	4.0	>16
8d	Phenyl	4-picolinylamine	4.0	2.0	1.0	1.0	>16
8e	H	4-picolinylamine	0.5	1.0	0.5	0.5	>16
9a	H	3-picolinylamine	1.0	2.0	2.0	0.5	8.0
9b	Methyl	3-picolinylamine	0.5	2.0	1.0	2.0	>16
9c	Isopropyl	3-picolinylamine	4.0	0.5	4.0	2.0	8
9d	Phenyl	3-picolinylamine	4.0	2.0	2.0	8.0	>16
9e	H	4-picolinylamine	0.5	2.0	0.5	0.5	>16
10a	H	4-picolinylamine	0.25	0.25	1.0	0.25	8.0
10b	Methyl	4-picolinylamine	0.125	0.5	0.25	0.125	2.0
10c	Isopropyl	4-picolinylamine	0.25	0.25	1.0	2.0	>16
10d	Phenyl	4-picolinylamine	1.0	1.0	2.0	4.0	>16
10e	H	4-picolinylamine	0.125	0.25	0.5	0.25	4.0
11a	H	3-picolinylamine	0. 5	2.0	4.0	0.5	>16
11b	Methyl	3-picolinylamine	0.25	0.5	2	0. 25	8.0
11c	Isopropyl	3-picolinylamine	0.125	0.5	0.25	2.0	4.0
11d	Phenyl	3-picolinylamine	4.0	1.0	2.0	4.0	>16
11e	H	3-picolinylamine	0.25	0.5	0.5	0.25	8.0
12		3-picolinylamine	2.0	2.0	2.0	0.5	>16
13		4-picolinylamine	0.5	0.5	0.25	1.0	>16
14		3-picolinylamine	1.0	2.0	1.0	0.5	8.0
15		4-picolinylamine	0.25	0.125	2.0	1.0	8.0
Fluconazole			0.5	0.5	1.0	0.5	>16
Naftifine			1.0	0.5	0.5	1.0	4.0

Abbreviations: ***C. alb.***, *Candida albicans* (ATCC 10231); ***C. gla.***, *Candida glabrata* (ATCC 0001); ***C. kru.***, *Candida krusei* (ATCC 6258); ***C. tro.***, *Candida tropicalis* (ATCC 1369); ***A. fum.***, *Aspergillus fumigatus* (KM8001).

The antifungal activities of target compounds were listed in **Table 1** and **Table 2**. It is obvious that all target compounds showed antifungal activity. Although some of compounds such as **8d**, **9c**, **9d**, **11d**, and **12** showed the weaker antifungal activity than that of the positive control drug (naftifine), most of compounds exhibited the potent activity against *C. albicans*, *C. glabrata*, *C. krusei*, and *C. tropicalis* with MIC values in the range of 0.125-4.0 μg/mL. Interestingly, the inhibitory activity of target

compounds **8a-c**, **8e**, **9a-b**, **9e**, **10a-e**, **11a-c**, **11e**, **13-15**, and **16-20** on *Candida albicans* are superior or closer to those of the reference drugs (fluconazole, naftifine). Of these, compounds **8a**, **10a**, **10c**, and **17** had better inhibitory effect than the control drugs, but their inhibitory effect on *Aspergillus fumigatus* is not ideal. Compounds **10b**, **10e**, and **11c** have broader antimicrobial spectrum, they can inhibit not only *Candida*, but also *A. fum*. Especially the compound **10b** showed excellent antifungal activities with MIC values in the range of 0.125-2 μg/mL.

Table 2. *In vitro* antifungal activities of the target compounds (MIC, μg/mL).

Compd	R	Nitrogen-containing groups	MIC, μg/mL				
			C.alb.	***C.gla.***	***C.kru.***	***C.tro.***	***A.fum.***
16	Isopropyl	Imidazole	0.5	1.0	0.25	1.0	>16
17	Isopropyl	Imidazole	0.25	0.5	1.0	1.0	>16
19	Benzylamino	Imidazole	1.0	0.5	0.5	2.0	>16
20	Benzylamino	Imidazole	0.5	2.0	2.0	0.5	8.0
Fluconazole			0.5	0.5	1.0	0.5	>16
Naftifine			1.0	0.5	0.5	1.0	4.0

Abbreviations: ***C. alb.***, *Candida albicans* (ATCC 10231); ***C. gla.***, *Candida glabrata* (ATCC 0001); ***C. kru.***, *Candida krusei* (ATCC 6258); ***C. tro.***, *Candida tropicalis* (ATCC 1369); ***A. fum.***, *Aspergillus fumigatus* (KM8001).

Subsequently, we preliminarily analyzed the structure-activity relationship of target compounds. It should be mentioned that the change of main chain region has a certain effect on antifungal activity, the antifungal activity of target compounds containing the fragment of 2,3-dihydrobenzo[*b*][1,4]dioxin is better than the benzo[*d*][1,3] dioxole. At the same time, the pyridine group can also replace imidazole group to retain antifungal activity. It was worth noting that the activity of the compounds (**12-15**) did not improve significantly with the length shortening of intermediate linker. Moreover, the antifungal activity of compounds decreased with the increase of R group volume. They did not show obvious inhibitory effect on *Aspergillus fumigatus*, when the R group of compounds is phenyl or phenylmethyl. The antifungal potency could be presented in the following order: **10b>10e>11c>8b>10a=11e >8a>9a>15>11b>14>9c>9b>8c>13>10c>9e>11a>12>8d>11d>9d>8c.**

2.4. In Vitro Antifungal Activity Against Fluconazole-Resistant Strains of C. alb

With the widespread application of fluconazole in clinical practice, the emergence of drug-resistant fungi has become more and more frequent. Therefore, it should be important to investigate the inhibitory activity of target compounds against fluconazole-resistant fungi. In this study, fluconazole-resistant strains of *C. alb.* (*strain 100* and *strain 103*) were selected as test strains. The preferred target compounds **10b**, **10e**, and **11c** were investigated the inhibitory effects on drug-resistant fungi, and the result was shown in **Table 3.**

The inhibition effect of fluconazole was not obvious against fluconazole-resistant strains of *C. alb.* (*strain 100* and *strain 103*), while naftifine could inhibit the fluconazole-resistant strains to some extent. At the same time, compounds **10b** and **11c** had significant inhibitory effect on *C. alb.* against fluconazole-resistant strains, and their MIC values were in the range of 0.5-2 μg/mL, while the inhibitory activity of compound **10e** was lower than that of compound **10b**, **11c**.

Table 3. *In vitro* antifungal activities of the target compounds (MIC, μg/mL) [a].

Compd	MIC, μg /ml	
	C.alb. Strain100	***C.alb. Strain103***
10b	0.5	2
10e	4	8
11c	2	2
Fluconazole	＞16	＞16
Naftifine	4	8

[a] **Abbreviations:** ***C. alb.***, *Candida albicans*; **Strain 100**, fluconazole-resistant strains of *Candida albicans*; **Strain 103**, fluconazole-resistant strains of *Candida albicans*; **Strain 100** and **strain 103** were provided by the Second Military Medical University.

2.5. Morphological Analysis of C. alb. Strains with Different Concentrations of Target Compounds

Observing the change of fungal cell density after administration is an important index to measure the efficacy of drugs. In the study, the untreated group and treated groups with positive control drugs (fluconazole, naftifine) and target compounds (**10b**, **11c**) were set, respectively. Their density was explored by polarizing microscopy in different drug concentrations (250 nm/mL, 50 nm/mL, and 5 nm/mL) (**Figure 2**).

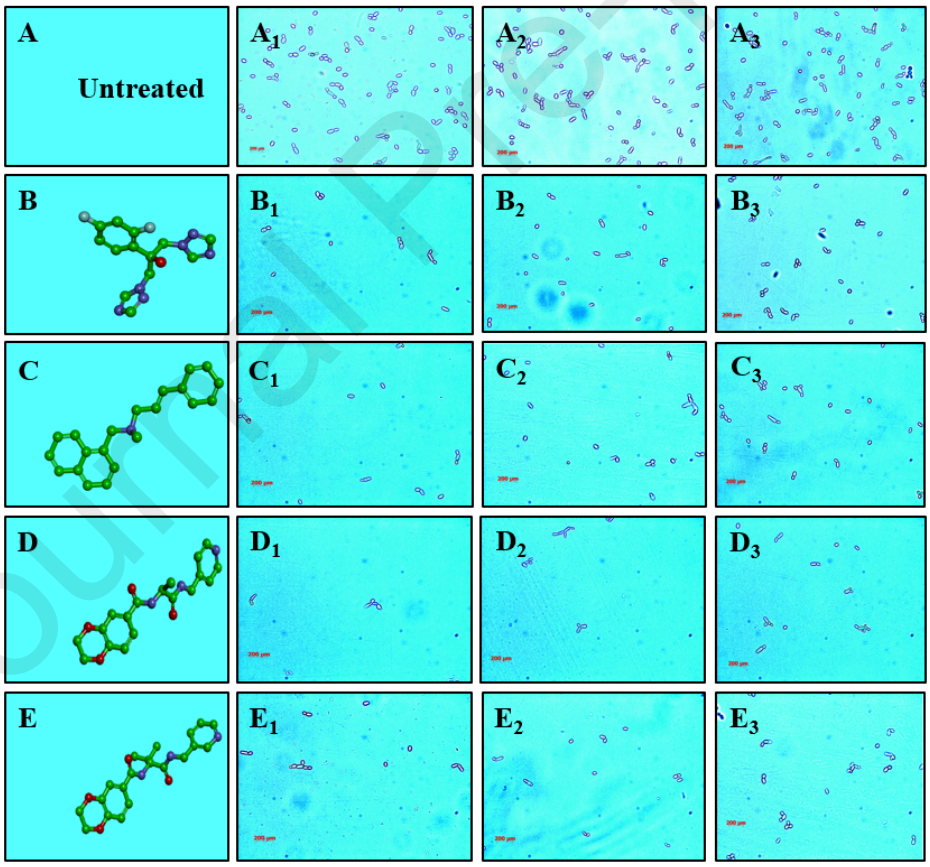

Figure 2. Polarizing microscopy results of target compounds and the positive control drugs against *Candida albicans* in different concentrations (**A_1-A_3**: 0 nm/mL; **B_1-E_1**: 250 nm/mL; **B_2-E_2**: 50 nm/mL; **B_3-E_3**: 5 nm/mL).

Candida albicans exhibited significant ability of cell proliferation in the untreated group, the density of fungal cells increased rapidly, and a large number of cell

germination and spores were observed around fungal cells. In the treated groups with high concentration (250 nm/mL), the proliferation of *Candida albicans* was inhibited, and the density of fungal cells was significantly lower than that of the untreated group. This phenomenon demonstrates that the antifungal efficacy of target compounds is consistent with the positive control drug, they not only effectively inhibited the cell division of *Candida albicans*, but also killed existing fungal cells. With the decrease of drug concentration to high concentration 50 nm/mL, the *Candida* density of treated group with positive control drugs (fluconazole, naftifine) increased, which indicated that the antifungal efficacy of control drugs has begun to weaken, and gradually reach critical nodes. However, the target compounds (**10b**, **11c**) still maintained good fungal inhibition ability at medium (50 nm/mL) / low (5 nm/mL) concentrations, and the density of fungal cells did not increase significantly, which was better than the treated group with positive control drugs (fluconazole, naftifine).

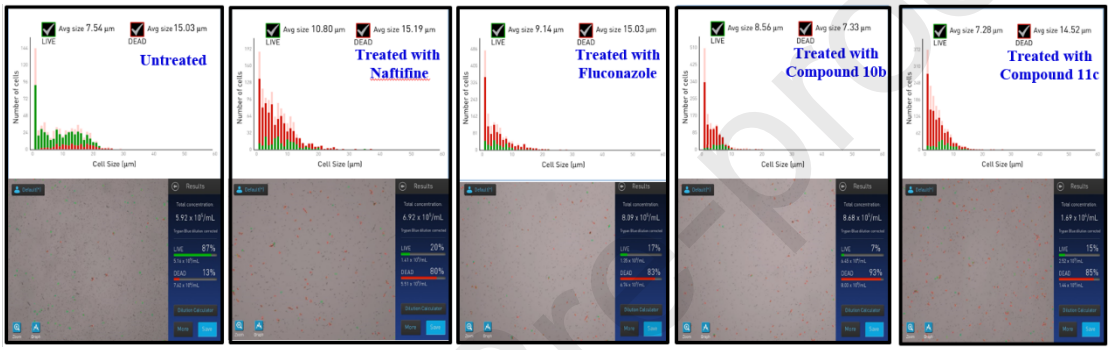

Figure 3. The results of *Candida albicans* survival rates in different treatment groups (untreated, naftifine, fluconazole, compound **10b**, and compound **10c**).

In order to further study the antifungal efficacy of target compounds (**10b**, **11c**). The survival rates of *Candida albicans* in different treatment groups were evaluated at the specific concentration (50 nm/mL). The results showed that the survival rate of fungal cells was as high as 87% in untreated group, and cell size exhibits the state of uniform distribution (**Figure 3**). In the treated groups with positive control drugs (naftifene, fluconazole) and target compounds (**10b**, **11c**), their survival rates of fungal cells falls to the range of 7%-20%. It is worth noting that the survival rates of fungal cells decreased to 7% and 15% in the treated groups with compounds **10b** and **11c**, and their values were even lower than that of the treated groups with positive control drugs (naftifene, 20%; fluconazole, 17%). At the same time, the cell size also also began to decline significantly. Therefore, the conclusion was obtained that compounds **10b** and **11c** can significantly affect the physiological functions of fungal cell, and inhibit their growth and reproduction .

2.6. Uptake of Target Compounds by Fungal Cells In Vitro

The uptake experiment of the small molecule probe and the target compounds in the fungal cell was performed by fluorescent microscope assay, and the possible uptake mechanism was presumed [31]. Lysol-Tracker Red can be used as cytoplasmic fluorescent dye, which can stimulate red fluorescence in the fungal cytoplasmic region. As can be seen from **Figure 4 A_1-C_1**, the red fluorescence distributes uniformly in the fungal cytoplasmic region, and it can also visually display the morphology and integrity

of fungal cells. At the same time, Hoechst 33258 was selected as non-inlaid human DNA fluorescent dye, which can dye the genetic material of fungal cells, and stimulate to produce blue fluorescence under the excitation of ultraviolet light. In the different treatment groups of fungal cells (**Figure 4 A_3-C_3**), the blue fluorescence is distributed in the central region of fungal cells, which indicates that Hoechst 33258 can locates the nucleus region of fungal cells. The target compounds can be stimulated to product the phenomenon of green fluorescence (**Figure 4 B_2-C_2**). When the fungal cells were treated with the target compounds **10b, 11c** for 8 h, the green fluorescence distributions were consistent with the Lysol-Tracker Red treatment group in the cytoplasmic region, which indicated that the target compounds mainly entered the cytoplasm to exert their pharmacological effects. In addition, the red and green fluorescence intensity of the treated groups (compounds **10b, 11c**) showed a gradual increasing trend in the cytoplasm (**Figure 4 A_4-B_4**). The possible reason is the target compounds destroy the permeability of fungal cells, and the exogenous fluorescent dyes can more easily enter the cytoplasm.

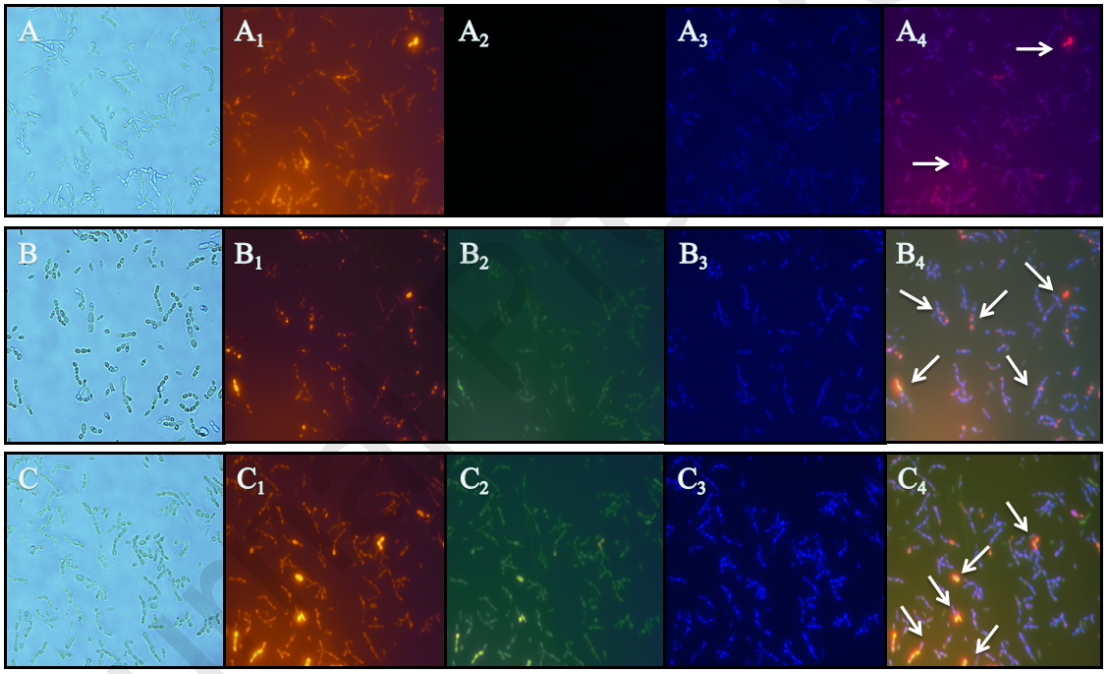

Figure 4. Fluorescence microscope images of *Candida albicans* (ATCC SC5314) cells after incubation with normal saline (A-A_4), target compound **10b** (5 μM) (B-B_4) and target compound 11c (5 μM) (C-C_4) as treatment groups for 8h. Red fluorescence (A_1-C_1) and blue fluorescence (A_3-C_3) are corresponding to Lysol-Tracker Red and Hoechst 33258, respectively. Green fluorescence (B_2-C_2) are corresponding to target compounds (**10b**, **11c**). Fluorescence overlay of each treatment group is shown in A_4-C_4.

2.7. The Observation Results of Transmission Electron Microscopy

In order to further visually understand the effect of target compound on the cell morphology of *Candida albicans*, the compound **10b** was selected as the representative test compound, and the structural changes of fungal cells were analyzed by transmission electron microscopy (TEM). At the early stage, the structure of *Candida albicans* cells mostly exists in the shape of ellipse. Fungal cell walls and membranes are located at

the edge of cells, which show the smooth and transparent characteristics. Cytoplasm and chromatin are evenly distributed in the inner region of fungal cells. At the same time, there is a clear boundary between the cells in the colony cell population, spores occur in some fungal cells, it can form new cell membranes and cell walls in the center of the original cells (**Figure 5 A_1-A_2**). When the treated group with compound **10b** was extended to the third day, the collapse of fungal cell wall and membrane began to appear, and some smooth surfaces changed into an irregular structure. At the same time, some specific phenomena occurred in the cytoplasmic regions, such as edema cavitation, disordered ridge arrangement, and exfoliation of rough endoplasmic reticulum particles (**Figure 5 B_1-B_2**). With the further increase of dosing time (7th day), the membrane of fungal cells began to break down, and the contents of cells continued to exudate. Ultimately, only residual fungal cell walls were left (**Figure 5 C_1-C_2**). The preliminary study demonstrated that the target compounds can destroy the surface of fungal cells, it can lead to the lysis and death of fungal cells.

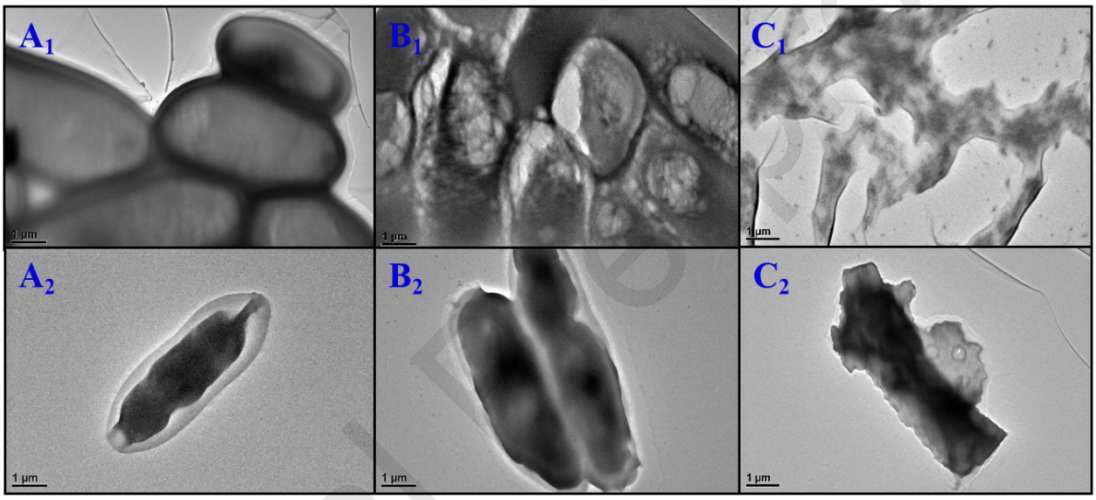

Figure 5. Transmission electron microscopy (SEM) results of target compound **10b** against *Candida albicans* (ATCC SC5314) in different time periods.

2.8. Heme Binding Studies of Target Compound 10b

In the synthetic pathway of fungal sterols, CYP51 as monooxygenase can catalyze 14α-methyl hydroxylation reaction of sterol precursors by using heme in the active chamber. Therefore, it is an important indicator to evaluate the binding ability of the target compound with heme, which can directly reflect the inhibitory effect of target compound on CYP51.

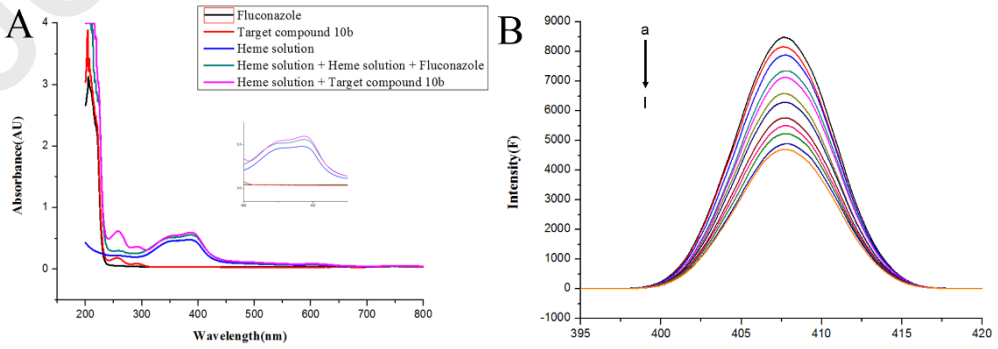

Figure 6. (A) UV-vis spectra of heme with compound **10b** and Fluconazole; **(B)**

Fluorescence spectra of heme in the absence and presence of compound **10b**.

In this study, the target compound **10b** with the best antifungal activity was selected as research object. Its binding ability with heme is tested via Ultraviolet-Visible (UV-vis) and fluorescence spectrum, which was depicted in **Figure 6 A, B**. In the UV-vis absorption spectrum, there is an absorption peak at 378.00 nm for heme solution, and fluconazole as the positive control drug and target compound **10b** did not exist ultraviolet absorption in the region. When the fluconazole and target compound **10b** were added into the heme solution, the absorption peak of heme solution showed an upward trend. The phenomenon indicates that the binding mode of target compound **10b** and heme is similar with fluconazole, they can cause changes in UV-vis spectrum by forming new complexes.

In the fluorescence spectrum, the target compound exhibits strong fluorescence excitation peaks at 408 nm. The fluorescence excitation peak showed a gradual decreasing trend with the increasing concentration of heme (0.0-50.0 nm/mL) in solution. This phenomenon further proves that target compound **10b** can bind to heme and exhibit strong binding ability. Since the fluorescence intensity is proportional to the target compound concentration, and their relationship can be expressed as

$$log(F0-F)/F=logKa+nlog[Q]$$

Where *[Q]* is the free concentration of a drug. *Ka* and *n* are the binding constant and the number of binding sites, respectively, which can be obtained from the linear plot of log *(F0-F)/F* versus log *[Q]* [32]. The binding energy (*Ka*) and the number of binding sites were calculated (n=1, Ka=1.11×10^6 M^{-1}) by the corresponding linear relationship. The results indicates that the nitrogen-containing arylamide derivatives can form the strong interaction with heme at a specific binding site.

2.9. Analysis of Sterol Composition in Candida albicans

In order to further determine the antifungal mechanism of the amidopyridine compounds (**10b**, **11c**), the sterol composition of *Candida albicans* were analyzed by *LC-MS* [16, 29]. The method has been successfully used to analyze the changes of sterol synthesis pathway in fungal cells, which can explain the action mechanism of fungal drug and the cause of fungal drug resistance. Fluconazole and naftifine were selected as the positive control drugs.

The analysis results were shown in **Table 4**. In the untreated control group, ergosterol account for 71.48% of the total sterol content. At the same time, lanosterol, eburicol and squalene were also observed, they accounted for 6.62%, 12.38%, 4.15%, respectively. In the treated group with fluconazole, ergosterol content sharply decreased to 4.74%, while lanosterol content increased significantly to 71.00%, and squalene was not detected in treatment group. These data indicate that fluconazole plays the antifungal role by inhibiting CYP51. In the treated group with naftifine, ergosterol content gradually decreased from 71.48% to 8.54%, and squalene content increased to 57.24%, while the eburicol content did not change significantly, which indicate that naftifine exerts the mainly antifungal activity by inhibiting SE. In the treated groups with target compounds **10b** and **11c**, these target compounds can result in the marked decreases in the ergosterol content. At the same time, eburicol content increased to

32.81% and 29.15%, squalene content increased to 43.69% and 40.14%. From the above analysis, the compounds **10b** and **11c** can exhibit two action mechanisms of fluconazole and naftifine. Therefore, the target compounds (**10b**, **11c**) can inhibit the double-target (SE, CYP51) activity, and synergistically block the biosynthesis pathway of ergosterol.

Table 4. Analysis of sterol composition in *C. albicans.*

Contents.	**% of total sterols (*Candida albicans*)**				
	Control	**Fluconazole (FLC)**	**Naftifine**	**Compound10b**	**Compound 11c**
Ergosterol	71.48	4.74	8.54	6.22	8.73
Lanosterol	6.62	20.82	17.21	10.27	14.68
Eburicol	12.38	71.00	11.63	32.81	29.15
Squalene	4.15	-	57.24	43.69	40.14
Unidentified	5.37	3.44	5.38	7.01	7.30

2.10. Antifungal Activity of Target Compunds 10b and 11c in vivo

In order to evaluate the pharmacodynamics of target compounds *in vivo*, animal test was performed. Compounds **10b** and **11c**, which have significant antifungal activity *in vitro*, were selected to evaluate their efficacy in mice. Fluconazole and naftifine were selected as the positive control drugs.

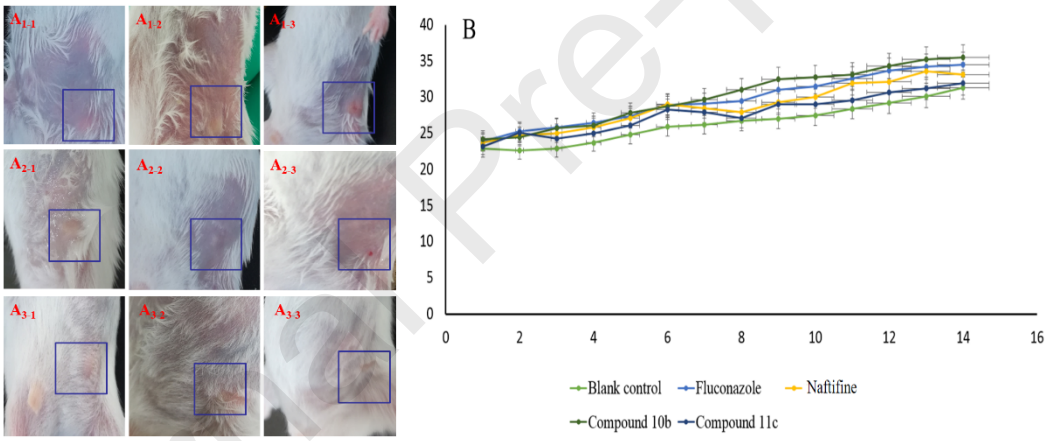

Figure 7. (A) The changes of fungal infection position in the treated groups with saline **(A_{1-1}-A_{1-3})**, compound **10b (A_{2-1}-A_{2-3})**, and compound **11c (A_{3-1}-A_{3-3})**; **(B)** The changes of mice weight during treatment.

First, the changes of fungal infection position and mice weight were evaluated during treatment time, which were shown in **Figure 7 A**, **B**. In the treated group with saline, the infected position of mice showed a gradual expansion trend with the prolongation of the treatment time, and the growth rate of mice weight was slower than that of these other treated groups with compounds **10b**, **11c**, fluconazole, and naftifine. In treated groups with compounds **10b**, **11c**, the infection positions showed the trend of gradual reduction, the infection positions completely disappeared and returned to the normal state at the 14th day. Subsequently, these mice were executed at the 15th day, the internal organs such as the heart, lung, liver, spleen, kidney, and fungal-infected tissues were removed, they were sectioned and *H/E* stained. These visceral tissue sections in the different treatment groups were selected and observed, they did not have significant differences in morphology, and the phenomenon of pathology has not been found

(**Figure 8**). Therefore, the conclusion was obtained that target compounds **10b**, **10c** can produce fungi-inhibiting effects *in vivo*, and they have less or no toxicity to normal visceral tissues.

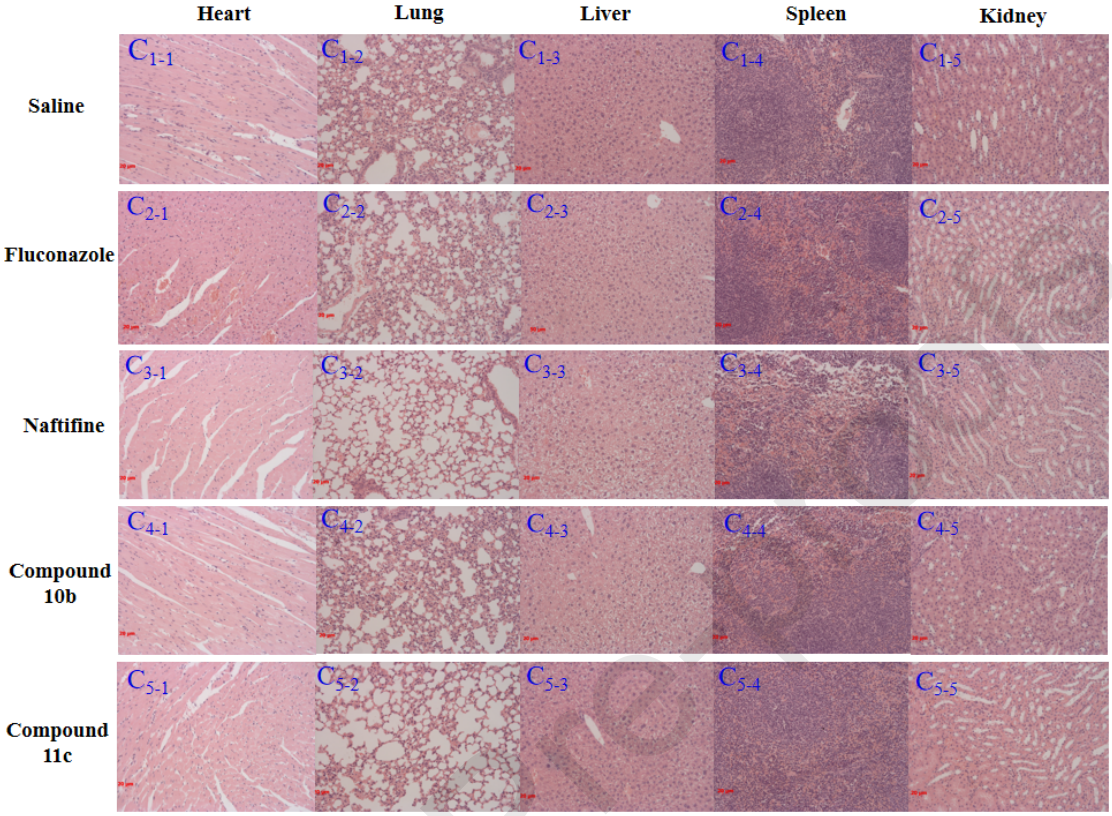

Figure 8. *H/E* staining of heart, lung, liver, spleen and kidney in different treatment groups (Saline, $C_{1\text{-}1}$-$C_{1\text{-}5}$; Fluconazole, $C_{2\text{-}1}$-$C_{2\text{-}5}$; Naftifine, $C_{3\text{-}1}$-$C_{3\text{-}5}$; Compound **10b**, $C_{4\text{-}1}$-$C_{4\text{-}5}$; Compound **11c**, $C_{5\text{-}1}$-$C_{5\text{-}5}$)

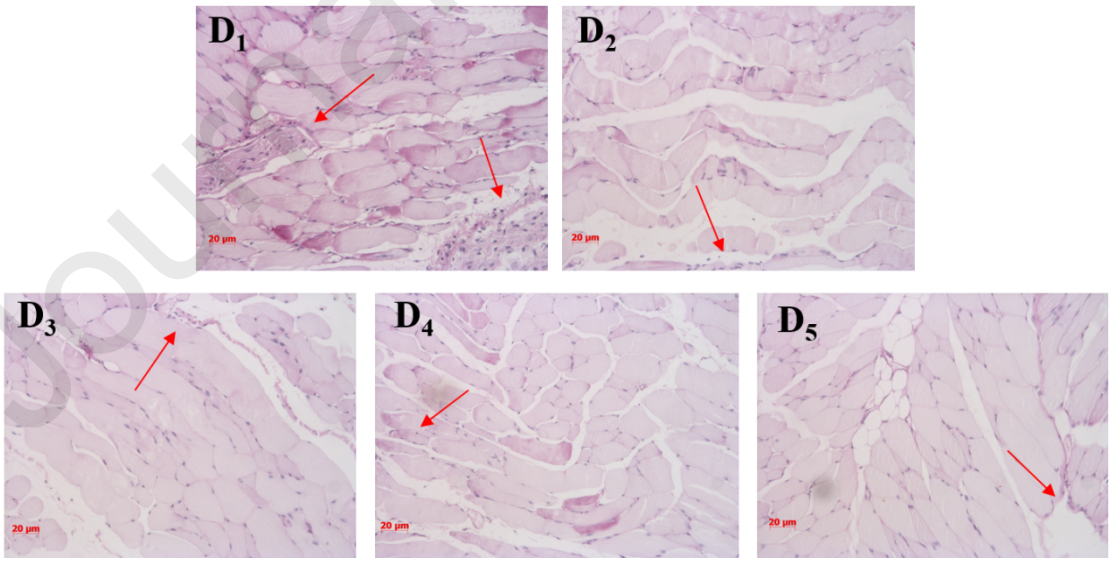

Figure 9. *H/E* staining of fungal infections tissues in different treatment groups (Saline, D_1; Fluconazole, D_2; Naftifine, D_3; Compound **10b**, D_4; Compound **11c**, D_5)

In order to further evaluate the effect of target compounds (**10b**, **11c**) on the fungal-infected tissues, the tissue sections were observed (**Figure 9**). In the treated group with

saline, a large amount of nuclear aggregation was found, which indicates that the region has developed a serious immune response, and the phenomenon was caused by pathogenic fungal infection. In the treated groups with positive control drugs and target compounds, these fungal-infected tissues have returned to their normal state, and the cell nuclear aggregation phenomenon disappeared at the infection region. This result suggested that the pathogenic fungi have been significantly inhibited, and the infected tissues have gradually returned to normal state. Therefore, the target compounds have the same antifungal activity as the positive drugs *in vivo*, and they can significantly inhibit the proliferation of fungi in mice with low toxicity.

2.11. Theoretical Evaluation of ADME/T Properties

Pharmacokinetic properties are very important indicators for improving the success rate of new drug development. Therefore, the ADME/T properties of target compounds were predicted (**Figure 10**) [17,24,27], and the prediction results were shown in **Figure 11.**

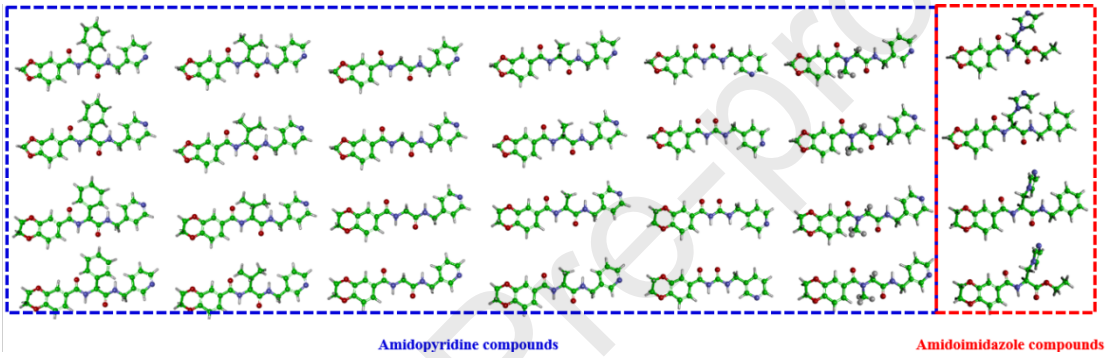

Figure 10. The structure of target compounds.

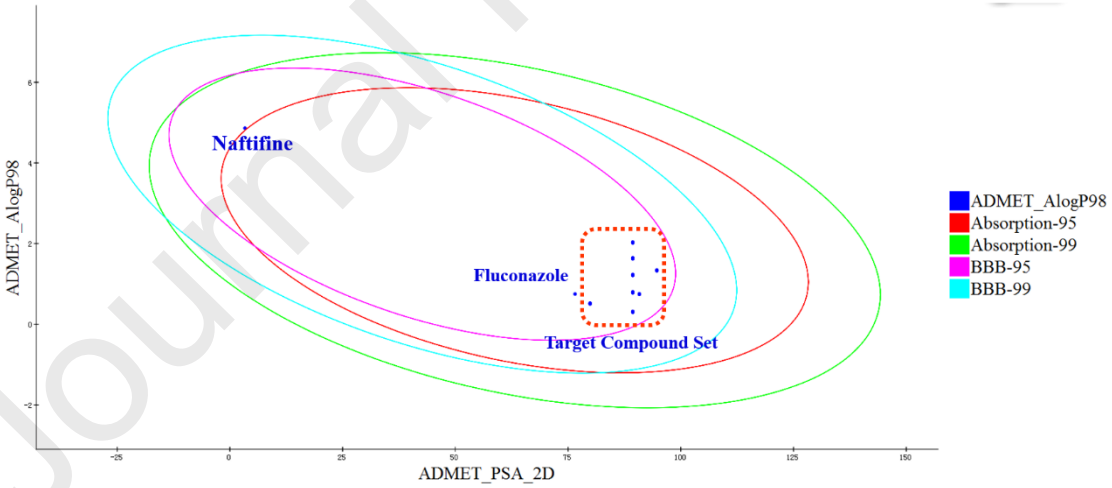

Figure 11. Plot of PSA versus Alog P for the target compounds. The 95% and 99% confidence limit ellipses that correspond to the blood-brain barrier and intestinal absorption models. Abbreviations: ADME/T, absorption, distribution, metabolism, excretion and toxicity; A log P, the logarithm of the partition cofficient between octanol and water; PSA, polar surface area; 2D, two-dimensional; BBB, blood brain barrier.

The two analogous 95% and 99% confidence ellipses for the blood-brain barrier (BBB) penetration and human intestinal absorption (HIA) models are represented in the biplot figure, respectively. All the target compounds and the control drug (fluconazole)

were positioned in the 99% confidence region for BBB penetration and HIA, and naftifine was excluded from the 95% confidence ellipses of HIA (Absorption-95), which indicate that the ADMET properties of target compounds exhibit appropriate reliability.

Table 5. *In silico* ADME/T prediction of the potential amidopyridine compounds and amidoimidazole compounds compared with the naftifine and fluconazole.

ADME/T parameters	Amidopyridine compounds	Amidoimidazole compounds	Naftifine	Fluconazole
A log *P*98 [a]	0.298~2.035	0.739~1.344	4.863	0.750
PSA[b]	89.343	90.811, 94.691	3.352	76.556
Aqueous solubility	3, 4	3	2	4
HIA[d]	0	0	1	0
PPB [e]	Highly bound	Highly bound	Highly bound	Highly bound
BBB penetration [f]	3	3	0	3
CYP450 2D6 binding [g]	0	0	0	1
Hepatotoxicity	Non-Toxic	Non-Toxic	Non-Toxic	Toxic
DTP [h]	Toxic, Non-Toxic	Toxic	Toxic	Toxic
FDA[i] rodent carcinogenicity	Non-carcinogen	Non-carcinogen	Non-carcinogen	Non-carcinogen
Ames mutagenicity	Non-mutagen	Non-mutagen	Non-mutagen	Non-mutagen
Aerobic biodegradability	Non-degradable, Degradable	Degradable	Non-degradable	Non-degradable
Skin sensitization	Non-irritant, Strong-sensitizer	Non-irritant, Strong-sensitizer	Strong-sensitizer	Strong-sensitizer
Skin irritating	Non-irritant or Mild-irritant	Non-irritant or Mild-irritant	Mild-irritant	Non-irritant

a. A log P98 (atom-based log *P*) (≦-2.0 or ≧7.0: very low absorption). **b.** PSA (polar surface area) (>150: very low absorption). **c.** Level of aqueous solubility predicted: 0 (extremely low), 1 (very low, but possible), 2 (low), 3 (good), 4 (optimal), 5 (too soluble), 6 (warning: molecules with one or more unknown A log *P* calculations). **d.** HIA (human intestinal absorption), level of human intestinal absorption prediction: 0 (good), 1 (moderate), 2 (poor), 3 (very poor). **e.** PPB, plasma protein binding. **f.** BBB (blood brain barrier), level blood brain barrier penetration prediction: 0 (very high penetrate), 1 (high), 2 (medium), 3 (low), 4 (undefined). **g.** Prediction cytochrome P4502D6 enzyme inhibition (0: non-inhibitor; 1: inhibitor). **h.** DTP, development toxicity potential. **i.** FDA, food and drug administration.

These detailed values of ADME/T properties were listed in **Table 5.** The key properties linked to drug bioavailability are A log*P* and PSA, respectively. Hydrophobicity of target compounds can be predicted and expressed with A log*P*. From this result, it can be seen that all A log*P* values are less than 5, which indicates that these compounds have proper absorption or permeation. The absorbed molecules with PSA<140 have high oral bioavailability, and these compounds are within this limit. Likewise, all of the compounds, except naftifine, exhibit good or optimal solubility levels for aqueous solubility, they can be effectively absorbed in the human intestine and highly bound to plasma proteins. Encouragingly, those target compounds can also remain the low-level BBB permeability and Non-Hepatotoxicity, and the CYP450 2D6 binding values is 0 (non-inhibitor), which indicates that target compounds can readily undergo oxidation and hydroxylation during the phase of metabolism. For toxicity risk,

these compounds are non-carcinogenic, non-mutagenic, degradable and non-irritating. Although some of compounds demonstrate a certain degree of DTP and Skin sensitization, further structural modifications may improve the compounds' toxicity profiles.

2.12. Molecular Docking

Molecular docking can provide the guide for further target structure-based compound optimization [33, 34]. In this study, the SE homology model and CYP51 protein crystal (PDB: 5V5Z) were selected as the docking target enzymes (SE and CYP51), compounds **10b**, **11c** and the positive control drugs (naftifine, fluconazole) were docked into the active sites. Images depicting the proposed binding modes were generated using PyMOL, and the docking results were showed in **Table 6** and **Figure 12**.

Table 6. Summary of the docking studies

Compd	-CDOCKER ENERGY	-CDOCKER INTERACTION ENERGY	Absolute Energy	Target Enzyme
10b	24.53	42.85	57.44	SE
11c	18.62	41.68	52.58	SE
Naftifine	21.15	39.92	49.51	SE
10b	34.65	47.72	60.67	CYP51
11c	36.37	45.38	56.62	CYP51
Fluconazole	27.72	44.76	65.94	CYP51

In the SE docking model, the energies of complex systems are reduced, and the binding energies of target compounds (**10b**, **11c**) (CDOCKER ENERGY: −24.53, −18.62 kcal/mol; CDOCKER INTERACTION ENERGY: −42.85, −41.68 kcal/mol) are close to naftifine (CDOCKER ENERGY: −21.15 kcal/mol; CDOCKER INTERACTION ENERGY: −39.92 kcal/mol), which reveal the target compounds could form the stable binding conformation with receptor SE. The docking conformations in active site of SE were displayed in **Figure 12 A_1, B_1**. It can be seen that the active chamber of SE exhibited a long column shape, compound **10b**, **11c** can properly match in the active chamber, and the various groups of target compounds can produce the interaction with the key amino acid residues around the active chamber. The 1,4-benzodioxan group of the compound **10b**, **11c** can bind to the internal region of active pocket, and form π-alkylation with Asp 329 and Ser330. In addition, the pyridine group can produce the hydrogen bonding interaction with Ile305 and Pro 307, respectively. At the same time, the compounds **10b**, **11c** can also be docked into the active chamber of the CYP51 (**Figure 12 A_2, B_2**). The CDOCKER ENERGY values were predicted as −34.65, −36.37 kcal/mol, and the CDOCKER INTERACTION ENERGY values were predicted as −47.72, −45.38 kcal/mol. Their docking energy is better than that of fluconazole (27.72 kcal/mol, 44.76 kcal/mol). This suggests that the target compounds can properly combine with CYP51 active cavity. The 1,4-benzodioxan group was surrounded by the key hydrophobic residues (Tyr 118, Leu 121, Tyr 132, Pro230, Leu376, His377, Ser 378, Ser 507, and Met 508), and it can produce the interaction of π-π and π-alkylation with Tyr 118, Leu 376, His 377, and Ser

507. The pyridine group of target compounds occupied the bottom region of the active cavity, which can form the key coordination bonds with heme iron ion (The coordinate bond length is 2.707 Å, 3.057Å). Additionally, the flexible branched chain contains the structure of amide bonds, which can form hydrogen bond interaction with Tyr 132. Therefore, the docking result can confirm that the target compounds can match well to the dual-target (SE, CYP51) binding cavity, and they can form the stable combination mode of dual-target. In addition, some alkane groups with appropriate size may be introduced into the region containing aryl fragment, which can increase the matching degree of target compounds with dual target enzymes.

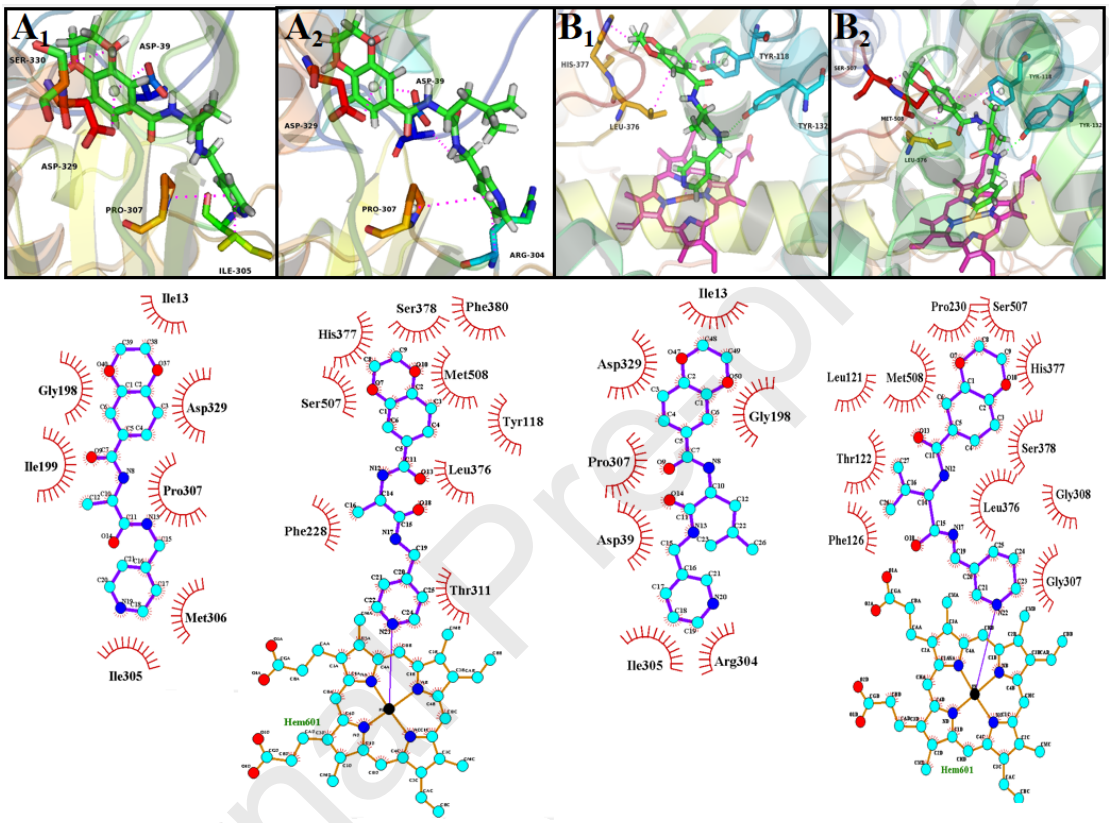

Figure 12. Docking models of representative compound **10b**, **11c**. **(A_1)** The molecular docking modeling of compound **10b** with SE; 2D molecular docking modeling of compound **10b** with SE. **(A_2)** The molecular docking model of compound **10b** with CYP51 binding site; 2D molecular docking model of compound **10b** with CYP51. **(B_1)** The molecular docking model of compound **11c** with SE; 2D molecular docking model of compound **11c** with SE. **(B_2)** The molecular docking model of compound **11c** with CYP51 binding site; 2D molecular docking model of compound **11c** with CYP51.

3. Conclusions

At present, the invasive phenomenon of pathogenic fungi and drug-resistant fungi is more and more frequent in clinical practice. The development of dual-target (SE and CYP51) antifungal inhibitors was chosen as an effective copy strategy. In this study, we first designed a series of amidoimidazole and amidopyridine target compounds based on the analysis of active sites (SE, CYP51) and the common pharmacophore features. Subsequently, the target compounds were synthesized, and corresponding antifungal activity was evaluated. Most of compounds demonstrate the potent

antifungal activity, especially compounds **10b** and **11c**, which not only had broad-spectrum antifungal activity, but also showed obvious inhibitory effect on drug-resistant fungi. Therefore, we continue to study its mechanism and evaluate its pharmacology *in vivo*. Preliminary studies have proved that these compounds can be absorbed by fungal cells, they mainly enter the cytoplasm to exert pharmacological effects, and ultimately cause the rupture of fungal cell membrane. At the same time, the target compounds can block ergosterol biosynthesis by inhibiting the activity of dual-target SE and CYP51. *In vivo* fungal invasion experiment on mice, these compounds also exhibited a certain antifungal activity against endogenous fungi with less side effects on animal visceral tissues. Finally, their ADME/T properties and molecular docking were performed, the result show that these target compounds can dock in the dual-target (SE, CYP51) binding sites with excellent pharmacokinetic properties. In summary, these studies demonstrate that target compounds have the potential to be developed as the lead compound.

4. Experimental section

4.1. General Methods for Chemistry

Unless otherwise noted, all commercial reagents and solvents were purchased and used without additional purification. Thin layer chromatography (TLC) analysis was performed on Silica Gel 60 F254 plates (Jiangyou, Yantai), which was used to monitor the reaction process. The silicagel (200-300 mesh) from Qingdao Ocean Chemicals (Qingdao, Shandong, China) was selected for column chromatography. The melting points of all compounds were determined and corrected with a Büchi Melting Point B-540 apparatus (Büchi Labortechnik, Flawil, Switzerland). Nuclear magnetic resonance (^{1}H-NMR and ^{13C}-NMR) spectra were recorded on a Bruker 600 MHz NMR spectrometer using TMS as an internal standard. Peak multiplicities were expressed as follows: s, singlet; d, doublet; t, triplet; q, quartet; dd, doublet of doublet; dt, doublet of triplet; td, triplet of doublet; ddd, doublet of doublet of doublet; m, multiplet; br, broad. The mass spectra (MS) were determined in ESI mode on an Shimadzu 8040 LC-MS (Shimadzu, Japan).

*4.2. General procedure for the synthesis of benzo[d][1,3]dioxole-5-carbaldehyde (**2a**) or2,3-dihydrobenzo[b][1,4]dioxine-6-carbaldehyde (**2b**)*

3,4-dihydroxybenzaldehyde (1.0 equiv) as the starting material and copper oxide (0.1 equiv) were added into DCM. Subsequently, dibromomethane (1.5 equiv) or dibromomethane (1.5 equiv) was continuously added to the mixed solution. The solution was heated to reflux for 40 minutes. After the reaction was completed, the mixed solution was filtered, and the solvent was removed by vacuum evaporation. The resulting product was dried to give the desired compound **(2a**, **2b)**.

*4.3. General procedure for the synthesis of quinoline-2-carboxylic acid (**3a-b**)*

Benzo[*d*][1,3]dioxole-5-carbaldehyde (**2a**; 1.0 equiv) or 2,3-dihydrobenzo[*b*] [1,4]dioxine-6-carbaldehyde (**2b**; 1.0 equiv) was added to the 2N/mL sodium hydroxide solution, and the mixture was stirred for 10 min. Subsequently, the potassium permanganate (2.0 equiv) was added to the reaction solution. The solution was heated to 80 °C for 6 h, and then cooled to room temperature. The solution was adjusted to pH=1-2 with the dilute hydrochloric acid solution. The white solid precipitate was

collected by filtration and dried to give the desired compound.

*4.4. General procedure for the synthesis of amino acid ethyl ester hydrochloride (**5a-d, 5-1, 5-2**)*

L-amino acids (Glycine, Alanine, Valine, Phenylglycine, Carbamic acid, Serine) (1.0 equiv) were dissolved in ethanol solution, respectively. Thionyl chloride (3.0 equiv) was slowly dripped into the mixed solution at 0 °C using ice salt bath. The mixture was heated to reflux for 3-6 h. Then, the reaction mixture was concentrated under reduced pressure to give the white solid **(5a-d**, **5-1**, and **5-2)**.

*4.5. General procedure for the synthesis of compounds (**6a-d, 6-1**,and **6-2**)*

The appropriate organic acids (benzo[*d*][1,3]dioxole-5-carboxylic acid, 2,3-dihydro -benzo[*b*][1,4]dioxine-6-carboxylic acid, 1 equiv) and HATU (1.2 equiv) were added in anhydrous DMF, respectively. The mixture was stirred at room temperature for 2 h. Then, amino acid ethyl ester hydrochloride (1.0 equiv) and DIEA (3.0 equiv) were added, the mixture was heated at 75 °C for 7 h. The reaction process was monitored by TLC analysis. After the completion of reaction, the reaction mixture was poured into ice water, and extracted with ethyl acetate, the organic phase was dried over Na_2SO_4 overnight. Finally, the desired compounds were obtained by vacuum distillation.

*4.6. General procedure for the synthesis of compounds (**6a-1**)*

The compounds (**6a**; 1.0 equiv), K_2CO_3 (3 equiv) and CH_3I (2 equiv) were dissolved in tetrahydrofuran. Then, the reaction mixture was stirred at 40 °C for 5 h. The reaction process was monitored by TLC analysis. After the completion of reaction, the mixture was poured into ice water, and extracted with ethyl acetate, the organic phase was dried over Na_2SO_4 overnight. Finally, the desired compounds were obtained by vacuum distillation.

*4.7. General procedure for the synthesis of compounds (**7a–e, 7–1**)*

The compounds (**6a-d**, **6a-1**, and **6-1**; 1.0 equiv) were dissolved in 15 mL methanol, the solution of 2N sodium hydroxide 30 ml was added. Then, the reaction mixture was stirred at 60 °C for 7 h. The reaction process was monitored by TLC analysis. After the completion of reaction, the methanol was removed by rotary evaporation, pH was adjusted to 2-3 by dilute hydrochloric acid solution, and white solid was filtered and dried to give the desired compounds.

*4.8. General procedure for the synthesis of compounds (**8a–e, 9a–e, 10a–e, 11a–e**, and **12-15**)*

The key intermediate (**7a–e**, **7–1**; 1.0 equiv) and PyBOP (1.2 equiv) were added into DMF, respectively. The mixture was stirred at room temperature for 2 h, then the pyridin-4-ylmethanamine or pyridin-3-ylmethanamine (1.2 equiv) and DIEA (3.0 equiv) were added, and the mixture was heated at 80 °C for 7 h. The reaction process was monitored by TLC analysis. After the completion of reaction, the reaction mixture was poured into ice water, and extracted with ethyl acetate, the organic phase was dried over Na_2SO_4 overnight, and the solvent was removed under vacuum. The resulting solid was dried to give the desired compounds. The crude product was purified by silica gel column chromatography (CH_2Cl_2: MeOH =100:3).

*4.9. General procedure for the synthesis of compounds (**16, 17**)*

The compound **6-2** (1 equiv), imidazole (2 equiv) and CDI (3 equiv) were added into

the anhydrous CH_3CN, respectively. The mixture was heated at 75 °C for 5 h. After the completion of reaction, the reaction mixture was poured into water, and then extracted with ethyl acetate. The organic layer was dried using Na_2SO_4, and evaporated under reduced pressure to give the desired production. The crude product was purified by silica gel column chromatography (CH_2Cl_2: MeOH =100:3).

*4.10. General procedure for the synthesis of compounds (**18-1, 18-2**)*

The compounds (**16**, **17**; 1 equiv) were dissolved in the 2N sodium hydroxide (30 mL) and methanol (15 mL) solution. Then, the reaction mixture was stirred at 60 °C for 2 h. The reaction process was monitored by TLC analysis. After the completion of reaction, the methanol was removed by rotary evaporation, pH was adjusted to 1-2 by the dilute hydrochloric acid solution, and white solid was filtered and dried.

*4.11. General procedure for the synthesis of compounds (**19, 20**)*

The key intermediate (**18-1**, **18-2**; 1 equiv) and PyBOP (1.2 equiv) were added into the solution of DMF, respectively. The reaction mixture was stirred at room temperature for 2 h. Then, the pyridin-4-ylmethanamine or pyridin-3-ylmethanamine (1.0 equiv) and DIEA (3 equiv) were added, the reaction mixture was heated at 80 °C, and stirred for 7 h. The reaction process was monitored by TLC analysis. After the completion of reaction, the reaction mixture was poured into ice water, the resulting solid was filtered and dried to give the desired compound. The crude product was purified by silica gel column chromatography (CH_2Cl_2: MeOH =100:3).

*4.12.1.N-(2-oxo-2-((pyridin-4-ylmethyl)amino)ethyl)benzo[d][1,3]dioxole-5-carboxamide (**8a**)*

The product was obtained as a white solid; yield: 71.5%; mp: 137.2–140.3℃. 1H NMR (500 MHz, DMSO) δ 9.02 (t, *J* = 5.6 Hz, 1H), 8.79 – 8.67 (m, 1H), 8.55 (d, *J* = 5.8 Hz, 2H), 7.68 – 7.43 (m, 2H), 7.34 (d, *J* = 5.5 Hz, 2H), 7.07 (d, *J* = 8.1 Hz, 1H), 6.16 (s, 2H), 4.52 (d, *J* = 5.9 Hz, 2H), 4.37 (d, *J* = 6.0 Hz, 2H).^{13}C NMR (126 MHz, DMSO) δ 166.07, 150.34, 149.99, 149.15, 147.87, 128.46, 122.79, 122.57, 108.40, 107.80, 102.18, 42.24, 41.56. ESI-MS m/z: 314 $[M+H]^+$; 336 $[M+Na]^+$. HPLC purity 99.1%. Retention time: 4.8 min, eluted with 20% purified water/80% methanol.

*4.12.2.N-(1-oxo-1-((pyridin-4-ylmethyl)amino)propan-2-yl)benzo[d][1,3]dioxole-5-carboxamide (**8b**)*

The product was obtained as a white solid: 69.1%; mp: 138.9–141.6℃. ^{1}H NMR (500 MHz, DMSO) δ 8.72 – 8.26 (m, 4H), 7.68 – 7.43 (m, 2H), 7.30 (d, *J* = 4.9 Hz, 2H), 7.00 (d, *J* = 8.1 Hz, 1H), 6.10 (s, 2H), 4.52 – 4.42 (m, 1H), 4.33 (d, *J* = 5.9 Hz, 2H), 1.38 (d, *J* = 7.2 Hz, 3H). ^{13}C NMR (126 MHz, DMSO) δ 173.43, 165.88, 149.39, 147.66, 128.50, 123.17, 122.53, 108.22, 108.17, 102.12, 49.78, 49.07, 41.58, 18.25. ESI-MS m/z: 328 $[M+H]^+$; 350 $[M+Na]^+$. HPLC purity 99.5%. Retention time: 4.7 min, eluted with 20% purified water/80% methanol.

*4.12.3.N-(3-methyl-1-oxo-1-((pyridin-4-ylmethyl)amino)butan-2-yl)benzo[d][1,3]dioxole-5-carboxamide (**8c**)*

The product was obtained as a white solid; yield: 71.6%; mp: 136.9–139.3℃. ^{1}H NMR (500 MHz, DMSO) δ 8.65 (t, *J* = 6.0 Hz, 1H), 8.48 (dd, *J* = 4.6, 1.4 Hz, 2H), 8.20 (d, *J* = 8.3 Hz, 1H), 7.57 – 7.36 (m, 2H), 7.27 (d, *J* = 5.8 Hz, 2H), 7.00 (d, *J* = 8.1 Hz, 1H), 6.10 (d, *J* = 1.8 Hz, 2H), 4.32 (qd, *J* = 16.4, 7.2 Hz, 3H), 2.15 (dq, *J* = 13.7, 6.8

Hz, 1H), 1.01 – 0.83 (m, 6H). ^{13}C NMR (126 MHz, DMSO) δ 172.07, 166.22, 150.20, 149.90, 148.94, 147.67, 128.60, 123.15, 122.59, 108.23, 108.20, 102.11, 59.93, 41.59, 30.18, 19.90, 19.46. ESI-MS m/z: 356 $[M+H]^+$; 378 $[M+Na]^+$. HPLC purity 100%. Retention time: 4.7 min, eluted with 10% purified water/80% methanol.

*4.12.4.N-(2-oxo-1-phenyl-2-((pyridin-4-ylmethyl)amino)ethyl)benzo[d][1,3]dioxole-5-carboxamide (**8d**)*

The product was obtained as a white solid; yield: 70.8%; mp: 140.7–142.1℃. ^{1}H NMR (500 MHz, DMSO) δ 8.84 (t, *J* = 5.8 Hz, 1H), 8.72 (d, *J* = 7.5 Hz, 1H), 8.46 (d, *J* = 5.7 Hz, 2H), 7.60 – 7.47 (m, 4H), 7.36 (dt, *J* = 24.8, 7.2 Hz, 3H), 7.20 (d, *J* = 5.7 Hz, 2H), 6.99 (d, *J* = 8.2 Hz, 1H), 6.13 – 6.07 (m, 2H), 5.70 (d, *J* = 7.5 Hz, 1H), 4.35 (d, *J* = 5.9 Hz, 2H). ^{13}C NMR (126 MHz, DMSO) δ 170.87, 165.90, 150.34, 149.52, 147.67, 138.61, 128.78, 128.33, 128.22, 123.42, 122.52, 108.34, 108.21, 102.14, 57.94, 41.72. ESI-MS m/z: 390 $[M+H]^+$; 412 $[M+Na]^+$. HPLC purity 100%. Retention time: 4.5 min, eluted with 20% purified water/80% methanol.

*4.12.5.N-methyl-N-(2-oxo-2-((pyridin-4-ylmethyl)amino)ethyl)benzo[d][1,3]dioxole-5-carboxamide(**8e**)*

The product was obtained as a white solid; yield: 67.2%; mp: 138.3–141.3℃. ^{1}H NMR (500 MHz, DMSO) δ 8.70 (s, *J* = 7.3 Hz, 1H), 8.50-8.48 (m, *J* = 15.6, 9.8 Hz, 2H), 7.45-7.42 (m, 2H), 7.27(d, *J* = 7.2 Hz, 2H), 6.94(d, *J* = 7.2 Hz, 1H), 6.03 (s, 2H),4.27 (s, 2H),3.88 (s, 2H),3.62 (s, 3H). ^{13}C NMR (126 MHz, DMSO) δ 170.87, 166.48, 149.37, 149.14, 146.58, 143.37, 127.37, 122.49, 121.52, 117.17, 116.99, 64.82, 64.47, 49.07, 43.38, 41.53. ESI-MS m/z: 326 $[M-H]^+$; 328 $[M+H]^+$; 350$[M+Na]^+$. HPLC purity 100%. Retention time: 4.9 min, eluted with 20% purified water/80% methanol.

*4.12.6.N-(2-oxo-2-((pyridin-3-ylmethyl)amino)ethyl)benzo[d][1,3]dioxole-5-carboxamide (**9a**)*

The product was obtained as a white solid; yield: 65.2%; mp: 136.9–140.3℃. ^{1}H NMR (500 MHz, DMSO) δ 8.95 (t, *J* = 5.6 Hz, 1H), 8.57 – 8.43 (m,3H), 7.71 (d, *J* = 7.8 Hz, 1H), 7.49 (dd, *J* = 7.4, 5.8 Hz, 1H), 7.43 (d, *J* = 5.6 Hz, 1H), 7.36 (dd, *J* = 7.8, 4.0 Hz, 1H), 7.10 – 6.89 (m, 1H), 6.10 (s, 2H), 4.47 (d, *J* = 5.8 Hz, 2H), 4.32 (d, *J* = 5.9 Hz, 2H).^{13}C NMR (126 MHz, DMSO) δ 169.80, 165.92, 149.29, 149.15, 148.52, 148.46, 147.83, 135.63, 135.57, 135.42, 128.55, 123.94, 123.83, 122.93, 122.74, 108.36, 108.29, 107.96, 107.77, 102.16, 43.30, 40.91. ESI-MS m/z: 314 $[M+H]^+$; 336 $[M+Na]^+$. HPLC purity 100%. Retention time: 4.8 min, eluted with 20% purified water/80% methanol.

*4.12.7.N-(1-oxo-1-((pyridin-3-ylmethyl)amino)propan-2-yl)benzo[d][1,3]dioxole-5-carboxamide (**9b**)*

The product was obtained as a white solid; yield: 66.4%; mp: 137.6–149.2℃. ^{1}H NMR (500 MHz, DMSO) δ 8.60 – 8.46 (m, 3H), 8.41 (d, *J* = 7.1 Hz, 1H), 7.70 (d, *J* = 7.8 Hz, 1H), 7.52 (d, *J* = 8.3 Hz, 1H), 7.48 (s, 1H), 7.39 (dd, *J* = 7.7, 4.9 Hz, 1H), 7.00 (d, *J* = 8.1 Hz, 1H), 6.10 (s, 2H), 4.49 – 4.42 (m, 1H), 4.38 – 4.28 (m, 2H), 1.35 (d, *J* = 7.2 Hz, 3H). ^{13}C NMR (126 MHz, DMSO) δ 173.23, 165.81, 150.19, 148.58, 148.05, 147.66, 135.74, 135.71, 128.53, 124.00, 123.13, 108.20, 108.15, 102.11, 56.50, 49.70,

18.21.ESI-MS m/z: 328 $[M+H]^+$; 350 $[M+Na]^+$. HPLC purity 100%. Retention time: 4.6 min, eluted with 20% purified water/80% methanol.

*4.12.8.N-(3-methyl-1-oxo-1-((pyridin-3-ylmethyl)amino)butan-2-yl)benzo[d][1,3]dioxole-5-carboxamide (**9c**)*

The product was obtained as a white solid; yield: 69.5%; mp: 138.4–140.6℃. ^{1}H NMR (500 MHz, DMSO) δ 8.62 (t, *J* = 5.8 Hz, 1H), 8.55 – 8.36 (m, 2H), 8.18 (d, *J* = 8.3 Hz, 1H), 7.66 (t, *J* = 10.5 Hz, 1H), 7.54 – 7.44 (m, 2H), 7.34 (dd, *J* = 7.7, 4.8 Hz, 1H), 6.99 (d, *J* = 8.1 Hz, 1H), 6.10 (d, *J* = 1.6 Hz, 2H), 4.33 (d, *J* = 5.9 Hz, 2H), 4.25 (t, *J* = 8.3 Hz, 1H), 2.13 (dq, *J* = 14.0, 6.8 Hz, 1H), 0.89 (dd, *J* = 20.0, 6.7 Hz, 6H). ^{13}C NMR (126 MHz, DMSO) δ 171.88, 166.13, 150.19, 149.15, 148.45, 147.67, 135.55, 135.41, 128.59, 123.86, 123.13, 108.22, 108.18, 102.11, 59.84, 30.26, 19.82, 5.1. ESI-MS m/z: 356 $[M+H]^+$; 378 $[M+Na]^+$. HPLC purity 99.1%. Retention time: 28.7 min, eluted with 20% purified water/80% methanol.

*4.12.9.N-(2-oxo-1-phenyl-2-((pyridin-3-ylmethyl)amino)ethyl)benzo[d][1,3]dioxole-5-carboxamide (**9d**)*

The product was obtained as a white solid; yield: 70.8%; mp: 141.4–144.7℃. ^{1}H NMR (500 MHz, DMSO) δ 8.81 (s, 1H), 8.67 (t, *J* = 33.0 Hz, 1H), 8.55 – 8.30 (m, 2H), 7.62 – 7.44 (m, 5H), 7.42 – 7.23 (m, 4H), 7.09 – 6.86 (m, 1H), 6.10 (s, 2H), 5.71 (t, *J* = 21.9 Hz, 1H), 4.47 – 4.24 (m, 2H). ^{13}C NMR (126 MHz, DMSO) δ 170.64, 165.81, 150.33, 149.05, 148.53, 147.68, 138.74, 135.31, 135.14, 128.75, 128.24, 128.15, 123.81, 123.38, 108.32, 108.21, 102.13, 57.80, 49.07. ESI-MS m/z: 390 $[M+H]^+$; 412 $[M+Na]^+$. HPLC purity 99.5%. Retention time: 4.4 min, eluted with 20% purified water/80% methanol.

*4.12.10.N-methyl-N-(2-oxo-2-((pyridin-3-ylmethyl)amino)ethyl)benzo[d][1,3]dioxole-5-carboxamide(**9e**)*

The product was obtained as a white solid; yield: 71.3%; mp: 139.4–141.3℃. ^{1}H NMR (500 MHz, DMSO) δ 8.70 (s, *J* = 7.3 Hz, 1H), 8.50-8.48 (m, *J* = 15.6, 9.8 Hz, 2H), 7.45-7.42 (m, 2H), 7.27(d, *J* = 7.2 Hz, 2H), 6.94(d, *J* = 7.2 Hz, 1H), 6.03 (s, 2H),4.27 (s, 2H),3.88 (s, 2H),3.62 (s, 3H). ^{13}C NMR (126 MHz, DMSO) δ 170.33, 166.38, 149.52, 149.02, 146.37, 143.04, 127.52, 122.45, 121.38, 116.57, 49.17, 43.34, 41.73. ESI-MS m/z: 328 $[M+H]^+$; 350$[M+Na]^+$. HPLC purity 98.4%. Retention time: 4.7 min, eluted with 20% purified water/80% methanol.

*4.12.11.N-(2-oxo-2-((pyridin-4-ylmethyl)amino)ethyl)-2,3-dihydrobenzo[b][1,4]dioxine-6-carboxamide (**10a**)*

The product was obtained as a white solid; yield: 71.9%; mp: 142.9–144.2℃. ^{1}H NMR (500 MHz, DMSO) δ 8.70 (t, *J* = 5.9 Hz, 1H), 8.59 – 8.41 (m, 3H), 7.47 – 7.39 (m, 2H), 7.27 (d, *J* = 5.9 Hz, 2H), 6.94 (d, *J* = 8.4 Hz, 1H), 4.32 (d, *J* = 6.2 Hz, 2H), 4.29 (d, *J* = 4.7 Hz, 2H), 3.90 (d, *J* = 5.9 Hz, 2H), 1.24 (s, 2H). ^{13}C NMR (126 MHz, DMSO) δ 170.02, 166.28, 149.87, 149.04, 146.58, 143.33, 127.52, 122.49, 121.37, 117.17, 116.99, 64.82, 64.47, 49.07, 43.30, 41.53. ESI-MS m/z: 326 $[M-H]^+$; 328 $[M+H]^+$; 350 $[M+Na]^+$. HPLC purity 99.7%. Retention time: 4.5 min, eluted with 20% purified water/80% methanol.

*4.12.12.N-(1-oxo-1-((pyridin-4-ylmethyl)amino)propan-2-yl)-2,3-dihydrobenzo[b][1,4] dioxine-6-carboxamide (**10b**)*

The product was obtained as a white solid; yield: 68.1%; mp: 141.2–144.9℃. ^{1}H NMR (500 MHz, DMSO-d_6) δ 8.59 – 8.32 (m, 4H), 7.52 – 7.36 (m, 2H), 7.25 (d, *J* = 5.8 Hz, 2H), 6.93 (d, J = 8.4 Hz, 1H), 4.46 (p, J = 7.2 Hz, 1H), 4.36 – 4.20 (m, 6H), 1.37 (d, J = 7.2 Hz, 3H). 13 C NMR (126 MHz, DMSO) δ 173.41 (s), 165.92 (s), 149.87 (s), 149.13 (s), 146.53 (s), 143.27 (s), 127.55 (s), 122.36 (s), 121.57 (s), 117.12 (d, J = 14.2 Hz), 64.83 (s), 64.47 (s), 49.69 (s), 41.53(s), 18.25 (s). ^{13}C NMR (126 MHz, DMSO-d_6) δ 173.41, 165.92, 149.87, 149.13, 146.53, 143.27, 127.55, 122.36, 121.57, 117.17, 117.06, 64.83, 64.47, 49.69, 41.53, 18.25. ESI-MS m/z: 340 $[M-H]^+$; 342 $[M+H]^+$; 364 $[M+Na]^+$. HPLC purity 99.2%. Retention time: 4.6 min, eluted with 20% purified water/80% methanol.

*4.12.13.N-(3-methyl-1-oxo-1-((pyridin-4-ylmethyl)amino)butan-2-yl)-2,3-dihydrobenzo[b][1,4]dioxine-6-carboxamide (**10c**)*

The product was obtained as a white solid; yield: 70.4%; mp: 145.1–147.8℃. ^{1}H NMR (500 MHz, DMSO) δ 8.62 (t, *J* = 6.0 Hz, 1H), 8.48 (d, *J* = 5.7 Hz, 2H), 8.19 (d, *J* = 8.4 Hz, 1H), 7.55 – 7.31 (m, 2H), 7.25 (t, *J* = 13.3 Hz, 2H), 6.93 (d, *J* = 8.4 Hz, 1H), 4.30 (ddd, *J* = 12.4, 9.2, 3.8 Hz, 7H), 2.15 (dq, *J* = 14.0, 6.8 Hz, 1H), 0.92 (dd, *J* = 12.6, 6.7 Hz, 6H). ^{13}C NMR (126 MHz, DMSO) δ 172.08, 166.24, 149.90, 148.96, 146.53, 143.29, 127.66, 122.58, 121.57, 117.15, 117.09, 64.83, 64.46, 59.87, 41.59, 30.15, 19.90, 19.45. ESI-MS m/z: 370 $[M+H]^+$; 392 $[M+Na]^+$. HPLC purity 99.7%. Retention time: 4.3 min, eluted with 20% purified water/80% methanol.

*4.12.14.N-(2-oxo-1-phenyl-2-((pyridin-4-ylmethyl)amino)ethyl)-2,3-dihydrobenzo[b][1,4]dioxine-6-carboxamide (**10d**)*

The product was obtained as a white solid; yield:67.8%; mp: 143.1–146.8℃. ^{1}H NMR (500 MHz, DMSO) δ 8.82 (t, *J* = 6.0 Hz, 1H), 8.72 (d, *J* = 7.6 Hz, 1H), 8.44 (d, *J* = 5.9 Hz, 2H), 7.55 – 7.46 (m, 4H), 7.41 – 7.32 (m, 3H), 7.16 (d, *J* = 5.8 Hz, 2H), 6.92 (d, *J* = 8.4 Hz, 1H), 5.69 (d, *J* = 7.6 Hz, 1H), 4.33 (d, *J* = 6.0 Hz, 2H), 4.11 (q, *J* = 5.3 Hz, 4H). ^{13}C NMR (126 MHz, DMSO) δ 170.86, 165.91, 149.87, 148.77, 146.68, 143.29, 138.70, 128.75, 128.31, 128.18, 127.30, 122.39, 121.75, 117.34, 117.08, 64.83, 64.45, 57.84. ESI-MS m/z: 404 $[M+H]^+$; 426 $[M+Na]^+$. HPLC purity 99.4%. Retention time: 4.6 min, eluted with 20% purified water/80% methanol.

*4.12.15.N-methyl-N-(2-oxo-2-((pyridin-4-ylmethyl)amino)ethyl)-2,3-dihydrobenzo[b][1,4]dioxine-6-carboxamide(**10e**)*

The product was obtained as a white solid; yield:67.8%; mp: 143.1–146.8℃. ^{1}H NMR (500 MHz, DMSO) δ 8.70 (t, *J* = 5.9 Hz, 1H), 8.49 (dd, *J* = 4.5, 1.5 Hz, 2H), 7.52 – 7.36 (m, 2H), 7.27 (d, *J* = 5.9 Hz, 2H), 6.94 (d, *J* = 8.4 Hz, 1H), 4.41 – 4.19 (m, 6H), 3.90 (d, *J* = 5.9 Hz, 2H), 2.94 (s, 3H). ^{13}C NMR (126 MHz, DMSO) δ 183.39, 173.13, 165.72, 149.85, 149.13, 146.53, 143.27, 127.55, 122.36, 121.57, 117.17, 117.06, 64.83, 64.47, 49.69, 42.47, 26.17. ESI-MS m/z: 340 $[M-H]^+$; 342 $[M+H]^+$; 364 $[M+Na]^+$. HPLC purity 99.6%. Retention time: 4.7 min, eluted with 20% purified water/80% methanol.

*4.12.16.N-(2-oxo-2-((pyridin-3-ylmethyl)amino)ethyl)-2,3-dihydrobenzo[b][1,4]dioxine-6-carboxamide (**11a**)*

The product was obtained as a white solid; yield: 71.8%; mp: 143.1–145.7℃. ^{1}H NMR (500 MHz, DMSO) δ 8.66 (t, *J* = 5.9 Hz, 1H), 8.46 (ddd, *J* = 6.8, 6.2, 1.6 Hz,

3H), 7.66 (d, *J* = 7.8 Hz, 1H), 7.47 – 7.37 (m, 2H), 7.35 (dd, *J* = 7.8, 4.8 Hz, 1H), 6.93 (d, *J* = 8.4 Hz, 1H), 4.45 – 4.16 (m, 6H), 3.87 (d, *J* = 5.9 Hz, 2H). ^{13}C NMR (126 MHz, DMSO) δ 169.82 (s), 166.21 (s), 149.14 (s), 148.46 (s), 146.57 (s), 143.33 (s), 135.43 (d, *J* = 4.5 Hz), 127.54 (s), 123.82 (s), 121.35 (s), 117.16 (s), 116.97 (s), 64.82 (s), 64.47 (s), 43.25 (s). ESI-MS m/z: 326 $[M-H]^+$; 328 $[M+H]^+$; 350 $[M+Na]^+$. HPLC purity 99.1%. Retention time: 4.4 min, eluted with 20% purified water/80% methanol.

*4.12.17.N-(1-oxo-1-((pyridin-3-ylmethyl)amino)propan-2-yl)-2,3-dihydrobenzo[b][1,4]dioxine-6-carboxamide (**11b**)*

The product was obtained as a white solid; yield: 67.9%; mp: 142.3–144.6℃. ^{1}H NMR (500 MHz, DMSO) δ 8.55 – 8.33 (m, 4H), 7.65 (d, *J* = 7.8 Hz, 1H), 7.50 – 7.39 (m, 2H), 7.34 (dd, *J* = 7.8, 4.8 Hz, 1H), 6.92 (d, *J* = 8.4 Hz, 1H), 4.45 (t, *J* = 7.2 Hz, 1H), 4.35 – 4.23 (m, 6H), 1.34 (d, *J* = 7.2 Hz, 3H). ^{13}C NMR (126 MHz, DMSO) δ 173.22, 165.83, 148.99, 148.42, 146.53, 143.27, 135.52, 135.22, 127.56, 123.83, 121.55, 117.16, 117.05, 64.83, 64.47, 49.61, 18.27. ESI-MS m/z: 340 $[M-H]^+$; 342 $[M+H]^+$; 364 $[M+Na]^+$. HPLC purity 99.2%. Retention time: 4.4 min, eluted with 20% purified water/80% methanol.

*4.12.18.N-(3-methyl-1-oxo-1-((pyridin-4-ylmethyl)amino)butan-2-yl)-2,3-dihydrobenzo[b][1,4]dioxine-6-carboxamide (**11c**)*

The product was obtained as a white solid; yield: 71.5%; mp: 145.7–148.2℃.^{1}H NMR (500 MHz, DMSO) δ 8.59 (t, *J* = 5.9 Hz, 1H), 8.46 (dd, *J* = 24.7, 2.7 Hz, 2H), 8.16 (d, *J* = 8.4 Hz, 1H), 7.66 (d, *J* = 7.8 Hz, 1H), 7.56 – 7.39 (m, 2H), 7.34 (dd, *J* = 7.8, 4.8 Hz, 1H), 6.92 (d, *J* = 8.4 Hz, 1H), 4.54 – 4.14 (m, 7H), 2.13 (dq, *J* = 13.9, 6.8 Hz, 1H), 0.88 (dd, *J* = 18.2, 6.7 Hz, 6H). ^{13}C NMR (126 MHz, DMSO) δ 171.89, 166.15, 149.20, 148.50, 146.52, 143.29, 135.47, 135.39, 127.66, 123.83, 121.54, 117.14, 117.08, 64.82, 64.46, 59.77, 49.07, 30.24, 19.83, 19.43. ESI-MS m/z: 370 $[M+H]^+$; 392 $[M+Na]^+$. HPLC purity 99.6%. Retention time: 4.5 min, eluted with 20% purified water/80% methanol.

*4.12.19.N-(2-oxo-1-phenyl-2-((pyridin-3-ylmethyl)amino)ethyl)-2,3-dihydrobenzo[b][1,4]dioxine-6-carboxamide (**11d**)*

The product was obtained as a white solid; yield: 68.9%; mp: 143.1–146.8℃. ^{1}H NMR (500 MHz, DMSO) δ 8.80 (s, 1H), 8.71 (d, *J* = 7.7 Hz, 1H), 8.43 (d, *J* = 4.6 Hz, 2H), 7.58 (d, *J* = 7.8 Hz, 1H), 7.52 – 7.45 (m, 4H), 7.33 (ddd, *J* = 12.8, 11.2, 6.0 Hz, 4H), 6.92 (d, *J* = 8.4 Hz, 1H), 5.67 (d, *J* = 7.7 Hz, 1H), 4.34 (d, *J* = 3.1 Hz, 2H), 4.30 – 4.26 (m, 4H). ^{13}C NMR (126 MHz, DMSO) δ 170.66, 165.83, 149.05, 148.53, 146.67, 143.29, 138.79, 135.31, 135.15, 128.73, 128.23, 128.12, 127.30, 123.81, 121.73, 117.32, 117.08, 64.83, 64.45, 57.72. ESI-MS m/z: 404 $[M+H]^+$; 426 $[M+Na]^+$. HPLC purity 99.2%. Retention time: 4.6 min, eluted with 20% purified water/80% methanol.

*4.12.20.*N-methyl-N-(2-oxo-2-((pyridin-3-ylmethyl)amino)ethyl)-2,3-dihydrobenzo[b][1,4]dioxine-6-carboxamide*(**11e**)*

The product was obtained as a white solid; yield:68.9%; mp: 141.4–145.8℃. ^{1}H NMR (500 MHz, DMSO) δ 8.71 (t, *J* = 5.9 Hz, 1H), 8.47 (dd, *J* = 4.5, 1.5 Hz, 2H), 7.52 – 7.34 (m, 2H), 7.26 (d, *J* = 5.9 Hz, 2H), 6.94 (d, *J* = 8.4 Hz, 1H), 4.41 – 4.37 (m, 6H), 3.89 (d, *J* = 5.9 Hz, 2H), 2.94 (s, 3H). ^{13}C NMR (126 MHz, DMSO) δ 181.92, 173.41, 165.29, 149.87, 149.13, 146.53, 143.06, 127.59, 122.13, 121.36, 117.17, 117.57, 64.69,

64.47, 49.41, 41.53, 23.83.ESI-MS m/z: 342 $[M+H]^+$; 364 $[M+Na]^+$. HPLC purity 98.9%. Retention time: 4.7 min, eluted with 20% purified water/80% methanol.

*4.12.21.N-((pyridin-4-ylmethyl)carbamoyl)benzo[d][1,3]dioxole-5-carboxamide (**12**)*

The product was obtained as a white solid; yield: 70.1%; mp: 135.5–137.1℃.^{1}H NMR (500 MHz, DMSO) δ 8.96 (s, 1H), 8.50 (d, *J* = 5.9 Hz, 2H), 7.68 – 7.40 (m, 2H), 7.29 (d, *J* = 5.8 Hz, 2H), 7.01 (d, *J* = 8.1 Hz, 1H), 6.10 (s, 2H), 4.47 (d, *J* = 5.9 Hz, 2H), 4.35 (s, 1H). 13C NMR (126 MHz, DMSO) δ 166.24, 151.23, 149.73, 148.92, 147.54, 137.45, 128.97, 123.55, 122.74, 108.33, 107.75, 103.45, 40.93. ESI-MS m/z: 300 $[M+H]^+$; 322 $[M+Na]^+$. HPLC purity 99.2%. Retention time: 5.5 min, eluted with 20% purified water/80% methanol.

*4.12.22.N-((pyridin-3-ylmethyl)carbamoyl)benzo[d][1,3]dioxole-5-carboxamide (**13**)*

The product was obtained as a white solid; yield: 65.9%; mp: 136.9–139.5℃. ^{1}H NMR (500 MHz, DMSO) δ 8.92 (s, 1H), 8.54 (d, *J* = 1.3 Hz, 1H), 8.45 (dd, *J* = 4.7, 1.5 Hz, 1H), 7.70 (d, *J* = 7.8 Hz, 1H), 7.48 (dd, *J* = 8.2, 1.6 Hz, 1H), 7.42 (d, *J* = 1.4 Hz, 1H), 7.35 (dd, *J* = 7.8, 4.8 Hz, 1H), 6.99 (d, *J* = 8.1 Hz, 1H), 6.09 (s, 2H), 4.47 (d, *J* = 5.9 Hz, 2H), 4.35 (d, *J* = 0.8 Hz, 1H).^{13}C NMR (126 MHz, DMSO) δ 165.94, 150.27, 149.29, 148.52, 147.83, 135.63, 135.57, 128.57, 123.93, 122.74, 108.35, 107.78, 102.15, 40.92. ESI-MS m/z: 300 $[M+H]^+$; 322 $[M+Na]^+$. HPLC purity 98.7%. Retention time: 5.4 min, eluted with 20% purified water/80% methanol.

*4.12.23.N-((pyridin-4-ylmethyl)carbamoyl)-2,3-dihydrobenzo[b][1,4]dioxine-6-carboxamide (**14**)*

The product was obtained as a white solid; yield: 67.8%; mp: 141.2–143.8℃. ^{1}H NMR (500 MHz, DMSO) δ 8.94 (t, *J* = 5.9 Hz, 1H), 8.49 (dd, *J* = 4.6, 1.3 Hz, 2H), 7.57 – 7.36 (m, 2H), 7.27 (d, *J* = 5.9 Hz, 2H), 6.94 (d, *J* = 8.3 Hz, 1H), 5.75 (s, 1H), 4.46 (d, *J* = 6.0 Hz, 2H), 4.34 – 4.22 (m, 4H).^{13}C NMR (126 MHz, DMSO) δ 166.10, 149.97, 149.21, 146.67, 143.46, 127.49, 122.55, 121.22, 117.30, 116.79, 64.83, 64.48, 42.18. ESI-MS m/z: 314 $[M+H]^+$; 336 $[M+Na]^+$. HPLC purity 99.6%. Retention time: 4.7 min, eluted with 20% purified water/80% methanol.

*4.12.24.N-((pyridin-3-ylmethyl)carbamoyl)-2,3-dihydrobenzo[b][1,4]dioxine-6-carboxamide (**15**)*

The product was obtained as a white solid; yield: 72.5%; mp: 135.9–137.5℃. ^{1}H NMR (500 MHz, DMSO) δ 8.95 (t, *J* = 5.9 Hz, 1H), 8.52 (dd, *J* = 4.6, 1.3 Hz, 2H), 7.48 – 7.41 (m, 2H), 7.28 (d, *J* = 5.9 Hz, 2H), 6.94 (d, *J* = 8.3 Hz, 1H), 5.74 (s, 1H), 4.46 (d, *J* = 6.0 Hz, 2H), 4.33 – 4.22 (m, 4H).^{13}C NMR (126 MHz, DMSO) δ 166.11, 152.21, 149.91, 146.62, 143.46, 127.47, 122.59, 121.22, 117.30, 116.79, 64.83, 64.47, 43.15. ESI-MS m/z: 314 $[M+H]^+$; 336 $[M+Na]^+$. HPLC purity 99.7%. Retention time: 4.6 min, eluted with 20% purified water/80% methanol.

*4.12.25. Ethyl 2-(1,3-dihydroisobenzofuran-5-carboxamido)-3-(1H-imidazol-1-yl) propanoate (**16**)*

The product was obtained as a white solid; yield: 69.4%; mp: 136.3–139.2℃. ^{1}H NMR (500 MHz, DMSO) δ 8.76 (d, J = 7.9 Hz, 1H), 7.63 (d, J = 20.0 Hz, 2H), 7.39 (dd, J = 8.1, 1.6 Hz, 1H), 7.31 (d, J = 1.6 Hz, 1H), 7.18 (s, 1H), 6.84 (s, 1H), 6.10 (s, 2H), 4.75 (ddd, J = 9.6, 8.1, 5.0 Hz, 1H), 4.49 (dd, J = 14.0, 5.0 Hz, 1H), 4.36 (dd, J = 14.0, 9.8 Hz, 1H), 4.13 (q, J = 7.1 Hz, 2H), 1.18 (t, J = 7.1 Hz, 3H).^{13}C NMR (126

MHz, DMSO) δ 170.15, 166.15, 150.56, 147.85, 138.27, 135.60, 128.79, 127.84, 122.97, 120.32, 108.40, 107.78, 102.24, 61.48, 54.28, 46.27, 14.45. ESI-MS m/z: 330 $[M+H]^+$; 352 $[M+Na]^+$. HPLC purity 99.6%. Retention time: 4.7 min, eluted with 20% purified water/80% methanol.

*4.12.26. Ethyl 2-(2,3-dihydrobenzo[b][1,4]dioxine-6-carboxamido)-3-(1H-imidazol -1-yl) propanoate (**17**)*

The product was obtained as a white solid; yield: 71.8%; mp: 141.6–144.2℃. ^{1}H NMR (500 MHz, DMSO) δ 8.75 (d, *J* = 7.9 Hz, 1H), 7.60 (s, 1H), 7.32 (dd, *J* = 11.5, 2.0 Hz, 2H), 7.18 (s, 1H), 6.93 (d, *J* = 8.2 Hz, 1H), 6.84 (s, 1H), 4.81 – 4.67 (m, 1H), 4.56 – 4.34 (m, 2H), 4.31 – 4.26 (m, 4H), 4.13 (q, *J* = 7.1 Hz, 2H), 1.18 (t, *J* = 7.1 Hz, 3H). ^{13}C NMR (126 MHz, DMSO) δ 170.17, 166.18, 146.89, 143.41, 138.25, 128.75, 126.85, 121.34, 120.32, 117.33, 116.81, 64.84, 64.48, 61.47, 54.19, 46.24, 14.46. ESI-MS m/z: 344 $[M+H]^+$; 366 $[M+Na]^+$. HPLC purity 99.8%. Retention time: 4.5 min, eluted with 20% purified water/80% methanol.

*4.12.27.N-(1-(benzylamino)-3-(1H-imidazol-1-yl)-1-oxopropan-2-yl)benzo[d][1,3]dioxole-5-carboxamide (**19**)*

The product was obtained as a white solid; yield: 69.9%; mp: 145.3–147.8℃. ^{1}H NMR (500 MHz, DMSO) δ 8.74 – 8.60 (m, 2H), 7.62 (s, 1H), 7.43 (d, *J* = 8.2 Hz, 1H), 7.37 (s, 1H), 7.32 (t, *J* = 7.5 Hz, 2H), 7.29 – 7.22 (m, 3H), 7.16 (s, 1H), 7.00 (d, *J* = 8.1 Hz, 1H), 6.82 (s, 1H), 6.10 (d, *J* = 3.6 Hz, 2H), 4.84 (td, *J* = 10.1, 4.3 Hz, 1H), 4.45 (dd, *J* = 13.9, 4.2 Hz, 1H), 4.30 (dt, *J* = 13.7, 8.3 Hz, 3H). ^{13}C NMR (126 MHz, DMSO) δ 169.60, 166.13, 150.39, 147.72, 139.50, 138.17, 128.74, 128.18, 127.64, 127.28, 123.08, 120.18, 108.29, 107.98, 102.18, 55.12, 47.32, 42.73. ESI-MS m/z: 344 $[M+H]^+$; 366 $[M+Na]^+$. HPLC purity 99.7%. Retention time: 4.5 min, eluted with 20% purified water/80% methanol.

*4.12.28.N-(1-(benzylamino)-3-(1H-imidazol-1-yl)-1-oxopropan-2-yl)-2,3-dihydrobenzo[b][1,4]dioxine-6-carboxamide (**20**)*

The product was obtained as a white solid; yield: 70.2%; mp: 150.3–152.8℃.^{1}H NMR (500 MHz, DMSO) δ 8.72 (s, 1H), 7.62 (d, *J* = 1.2 Hz, 1H), 7.43 – 7.38 (m, 1H), 7.38 – 7.33 (m, 2H), 7.34 – 7.28 (m, 2H), 7.29 – 7.21 (m, 3H), 7.17 (dd, *J* = 2.4, 1.1 Hz, 1H), 6.91 (d, *J* = 8.4 Hz, 1H), 6.81 (s, 1H), 4.84 (td, *J* = 10.2, 4.3 Hz, 1H), 4.45 (dd, *J* = 13.8, 3.9 Hz, 1H), 4.27 (d, *J* = 4.2 Hz, 3H), 3.45 – 3.42 (m, 4H). ^{13}C NMR (126 MHz, DMSO) δ 169.67, 166.15, 146.71, 143.30, 139.56, 138.17, 128.72, 128.66, 127.61, 127.25, 121.50, 120.18, 117.14, 117.02, 56.49, 55.19, 47.27, 42.70. ESI-MS m/z: 405 $[M-H]^+$. HPLC purity 99.2%. Retention time: 4.7 min, eluted with 20% purified water/80% methanol.

4.13. In Vitro Antifungal Activity Test

In order to detect the antifungal activity of target compounds, the vitro minimum inhibitory concentrations (MIC) was performed using the standard guidelines described in the National Committee for Clinical Laboratory Standards (NCCLS) [30]. The common pathogenic fungi in human body (*C. alb.*, *Candida albicans* (ATCC 10231); *C. gla.*, *Candida glabrata* (ATCC 0001); *C. kru*, *Candida krusei* (ATCC 6258); *C. tro.*, *Candida tropicalis* (ATCC 1369)) were considered as test strains. Fluconazole and naftifine were selected as positive control drugs. In this study, all of target compounds

and positive control drugs were dissolved in DMSO solvent， and they were serially dripped into the growth medium with different strains, and the concentration gradient of test compound was set to 0.03, 0.0625, 0.125, 0.5, 1, 2, 4, 8 and 16 ug/mL, respectively. Subsequently, they were statically cultured in a 35 °C incubator, and the MIC results were observed and recorded.

4.14. Fungal Cell Uptake and Intracellular Drug Release

Candida albicans (ATCC SC5314) cells were seeded into 8-well glass bottom plate with a density of 2×10^4 cells per well. After 24 h, the fungal cells were incubated with different ways (Untreated; Treated with compounds **10b**; Treated with compounds **11c**) for 8 h. Subsequently, these fungal cells of treatment groups were stained with nuclear stains (Hoechst 33342) and cytoplasmic stains (Lyso-Tracker Red) for 2 h, respectively. These samples of fungal cells were washed with PBS for 3 times, and examined using fluorescence microscope. Hoechst 33342 can be excited at 330nm~400nm nm (blue), target compounds can be excited at 420nm~485nm (green), Lyso-Tracker Red can be excited at 460nm~550nm (red).

4.15. The Experiment of Transmission Electron Microscopy (TEM)

According to the test protocol of NCCLS, the concentration of target compound **10b** in the bacterial solution was adjusted to 4 ug/mL, and they were incubated at 35℃. Subsequently, the bacterial solution was sampled at different time points (2d, 6d and 10d), and they were fixed in 4℃ refrigerators with 3% glutaric acid, washed with PBS solution. Finally, these samples were further stained with uranium osmium for 30 min, they were observed using transmission electron microscopy.

4.16. The Analysis Components Experiment of C. albicans Cells

In the study, *Candida albicans* (ATCC SC5314) was inoculated in Sabouraud medium, and cultured on a shaker (180 rpm, 35°C) for 16h. After two consecutive activation of fungal cells, the suspension of fungal cells was added to the culture medium, and the final concentration of control drugs and target compounds was set to 8 ug/mL. Continuous vibration culture for 16 h, the wet fungi (0.5 g) treated with different compounds were weighed, washed, centrifuged and saponify, the saponified solution was extracted with petroleum ether. After washing the organic solvent with saturated brine, the organic solvent was further removed by vacuum distillation. Finally, those samples were obtained, and detected by LC-MS. The LC-MS data were analysed using Shimadzu software (Shimadzu MSD productivity ChemStation for LC and LC/MS systems data analysis application) and matched to known MS data using the NIST Spectrum Database.

4.17. Determination of Fluorescence and UV Spectroscopy

In this fluorescence absorption experiment, the heme solution was set to (40 nm/mL), target compound (5.0 nm/mL) was added dropwise to the heme solution, and each group samples were incubated at 35℃ for 30 min. The emission spectrum of 530-575nm was recorded using 500 nm as excitation wavelength. The fluorescence intensity used in this paper is considered as the value after dilution effect.

In this Ultraviolet absorption experiment, the different experimental groups (blank control group, heme solution group, target compound group, fluconazole group, heme solution group + target compound group and heme + fluconazole group) were set up,

and incubated at 35℃ for 2 h. Subsequently, the sample solution of each group was absorbed and added into quartz dish. The emission spectrum was recorded using 383.00 nm and 608.00 nm as excitation wavelength.

4.18. In Vivo Therapeutic Efficacy

These mice with abdominal *Candida* infection were randomly divided into 5 groups: (1) Saline solution-injected group; (2) Fluconazole-injected group; (3) Naftifine-injected group; (4) Compound **10b**-injected group; (5) Compound **11c**-injected group. Therapy was continued through abdominal injection for 14 days. Finally, these mice tissues, including the heart, livers, spleen, lung, kidney, and endothelial tissue in abdominal infection, were harvested and collected immediately for *H/E* histology analysis. All of the animal experiments were conducted under approved protocols of the Institutional Animal Care and Use Committee of Liaocheng University.

4.19. ADME/T prediction

The failure rate of drug development is as high as 60% due to the poor pharmacokinetic properties and toxicity (ADME/T). Therefore, the prediction of ADMET value plays an important role in the development of novel target compounds. In the study, the target compounds were predicted using the DS ADMET program in Discovery Studio 3.5. The specific operation process was performed as follows: Frist, the small molecule compound files containing target compounds were imported. Then, the "ADMET descriptors" module was selected and opened, the prediction items (aqueous solubility, blood brain barrier penetration, CYP2D6 binding, hepatotoxicity, intestinal absorption and plasma protein binding) were set as research objects in the parameter browser, respectively. Finally, the program was run to obtain the corresponding results.

4.20. Molecular Docking

Molecular docking is an important analytical method, which can help us understand the binding mode of ligand and receptor. First, the target compound was optimized, which included adding all hydrogen atoms, checking the atom types and bond order, generating low energy ring conformations. Subsequently, the protein structure was prepared: All hydrogen atoms were added, water molecules around proteins was removed, their backbone and sidechain were adjusted and modified, missing residues and loop segments near the active sites were added using Prime. The binding region of co-crystallized ligand was selected as the active center of target enzyme (The Site Sphere of the SE homology model-grid is 21.3992, 35.7408, 23.7659, 13.5317; The position of the 5V5Z-grid is -37.5166, -17.4582,26.2275, 15.3922), and the parameter of active sphere was set to 9 Å. Then, the target compounds were docked into the active site using CDOCKER program. The pose cluster radius and random conformations were set to 10, and all other options remain the default during the parameter setting. Finally, the docking results were obtained.

Declaration of Competing Interest

The authors declare that they have no conflict of interest.

Acknowledgements

This work was supported by the National Natural Science Foundation of China (Grant No. 81703357, Grant No. 21473085, Grant No.31701827), the Shandong Provincial

Natural Science Foundation (Grant No. ZR2017BH102) and the Open Project of Shandong Collaborative Innovation Center for Antibody Drugs (Grant No. CIC-AD1837). This work was also supported by the Open Project of Shandong Collaborative Innovation Center for Antibody Drugs, and Tai-Shan Scholar Research Fund of Shandong Province of China. This work was also technically supported by Engineering Research Center for Nanomedicine and Drug Delivery Systems.

References

[1] D.A. Enoch, H.A. Ludlam, N.M. Brown, Invasive fungal infections: a review of epidemiology and management options, J. Med. Microbiol. 55 (2006) 809-818.

[2] G. Suleyman, G.J. Alangaden, Nosocomial Fungal Infections: Epidemiology, Infection Control, and Prevention, Infect. Dis. Clin. North. Am. 30 (2016) 1023- 1052.

[3] T.M. Gonzalez Santiago, B. Pritt, L.E. Gibson, N.I. Comfere, Diagnosis of deep cutaneous fungal infections: Correlation between skin tissue culture and histopathology, J. Am. Acad. Dermatol. 71 (2014) 293-301.

[4] A. Anighoro, J. Bajorath, G. Rastelli, Polypharmacology: challenges and opportunities in drug discovery, J. Med. Chem. 57 (2014) 7874-7887.

[5] Z. Jiang, Y. Wang, W. Wang, S. Wang, B. Xu, G. Fan, G. Dong, Y. Liu, J. Yao, Z. Miao, W. Zhang, C. Sheng. Discovery of highly potent triazole antifungal derivatives by heterocycle-benzene bioisosteric replacemen, Eur. J. Med. Chem. 64 (2013) 16-22.

[6] D. Zhao, S. Zhao, L. Zhao, X. Zhang, P. Wei, C. Liu, C. Hao, B. Sun, X. Su, M. Cheng, Discovery of biphenyl imidazole derivatives as potent antifungal agents: Design, synthesis, and structure-activity relationship studies, Bioorg. Med. Chem. 25 (2017) 750-758.

[7] C.M. Calvet, D.F. Vieira, J.Y. Choi, D. Kellar, M.D. Cameron, J.L. Siqueira- Neto, J. Gut, J.B. Johnston, L. Lin, S. Khan, J.H. McKerrow, W.R. Roush, L.M. Podust, 4-Aminopyridyl-Based Cyp51 Inhibitors as Anti-Trypanosoma Cruzi Drug Leads with Improved Pharmacokinetic Profile and *in Vivo* Potency, J. Med. Chem. 57 (2014) 6989-7005.

[8] B. Sun, W.X. Huang, M. Liu, Evaluation of the combination mode of azoles antifungal inhibitors with CACYP51 and the influence of site-directed mutation, J. Mol. Graph. Model. 73 (2017) 157-165.

[9] J. Nalawade, A. Shinde, A. Chavan, S. Patil, M. Suryavanshi, M. Modak, P. Choudhari, V.D. Bobade, P.C. Mhaske, Synthesis of new thiazolyl-pyrazolyl- 1,2,3-triazole derivatives as potential antimicrobial agents, Eur. J. Med. Chem. 179 (2019) 649-659.

[10] A. Jain, S. Jain, S. Rawat, Emerging fungal infections among children: A review on its clinical manifestations, diagnosis, and prevention, J. Pharm. Bioallied. Sci. 2 (2010) 314-320.

[11] H. Yousfi, S. Ranque, J.M. Rolain, F. Bittar, *In vitro* polymyxin activity against clinical multidrug-resistant fungi, Antimicrob. Resist. Infect. Control. 8 (2019) 66.

[12] S.C. Chen, M.A. Slavin, T.C. Sorrell, Echinocandin antifungal drugs in fungal infections: a comparison, Drugs. 71 (2011) 11-41.

[13] V. Moudgal, J. Sobel, Antifungals to treat Candida albicans, Expert. Opin.

Pharmacother. 11(2010) 2037-2048.
[14] M. Nowosielski, M. Hoffmann, L.S. Wyrwicz, P. Stepniak, D.M. Plewczynski, M. Lazniewski, K. Ginalski, L. Rychlewski, Detailed Mechanism of Squalene Epoxidase Inhibition by Terbinafine, J. Chem. Inf. Model. 51(2011) 455-462.
[15] W.J. Hoekstra, E.P. Garvey, W.R. Moore, S.W. Rafferty, C.M. Yates, R.J. Schotzinger, Design and optimization of highly-selective fungal CYP51 inhibitors, Bioorg. Med. Chem. Lett. 24 (2014) 3455-3458.
[16] S. Zhao, L. Zhao, X. Zhang, C. Liu, C. Hao, H. Xie, B. Sun, D. Zhao, M. Cheng, Design, synthesis, and structure-activity relationship studies of benzothiazole derivatives as antifungal agents, Eur. J. Med. Chem. 123 (2016) 514-522.
[17] B. Sun, H. Zhang, M. Liu, Z. Hou, X. Liu, Structure-based virtual screening and ADME/T-based prediction analysis for the discovery of novel antifungal CYP51 inhibitors, Medchemcomm. 9 (2018) 1178-1187.
[18] W.J. Hoekstra, E.P. Garvey, W.R. Moore, S.W. Rafferty, C.M. Yates, R.J. Schotzinger, Design and optimization of highly-selective fungal CYP51 inhibitors, Bioorg. Med. Chem. Lett. 24 (2014) 3455-3458.
[19] Pooja, P. Prasher, P. Singh, K. Pawar, K.S. Vikramdeo, N. Mondal, S.S. Komath, Synthesis of amino acid appended indoles: Appreciable anti-fungal activity and inhibition of ergosterol biosynthesis as their probable mode of action, Eur. J. Med. Chem. 80 (2014) 325-339.
[20] B. Sun, W. Huang, M. Liu, K. Lei, Comparison and analysis of the structures and binding modes of antifungal SE and CYP51 inhibitors, J. Mol. Graph. Model. 77 (2017) 1-8.
[21] X. Cao, Y. Xu, Y. Cao, R. Wang, R. Zhou, W. Chu, Y. Yang, Design, synthesis, and structure-activity relationship studies of novel thienopyrrolidone derivatives with strong antifungal activity against Aspergillus fumigates, Eur. J. Med. Chem.102 (2015) 471-476.
[22] S. Zhou, S.; Y. Li, T. Hou, Feasibility of Using Molecular Docking-Based Virtual Screening for Searching Dual Target Kinase Inhibitors, J. Chem. Inf. Model. 53 (2013) 982-996.
[23] A.S. Reddy, S. Zhang, Polypharmacology: drug discovery for the future, Expert. Rev. Clin. Pharmacol. 6 (2013) 41-47.
[24] R. Li, X. Su, Z. Chen, W. Huang, Y. Wang, K. Wang, B. Lin, J. Wang, M. Cheng, Structure-based virtual screening and ADME/T-based profiling for low molecular weight chemical starting points as p21-activated kinase 4 inhibitors, RSC Adv. 5 (2015) 23202-23209.
[25] J.Y. Choi, C.M. Calvet, S.S. Gunatilleke, C. Ruiz, M.D. Cameron, J.H. McKerrow, L.M. Podust, W.R. Roush, Rational Development of 4-Aminopyridyl-Based Inhibitors Targeting Trypanosoma cruzi CYP51 as Anti-Chagas Agents, J. Med. Chem. 56 (2013) 7651-7668.
[26] M.V. Papadopoulou, G.I. Bloomer, H.S. Lepesheva, M. Rosenzweig, M. Kaiser, B. Aguilera-Venegas, S.R. Wilkinson, E. Chatelain, J.R. Ioset, Novel 3- nitrotriazole-based amides and carbinols as bifunctional antichagasic agents, J. Med. Chem. 58 (2015) 1307-1319.

[27] B. Sun, Y. Dong, K. Lei, J. Wang, L. Zhao, M. Liu, Design, synthesis and biological evaluation of amide-pyridine derivatives as novel dual-target (SE, CYP51) antifungal inhibitors, Bioorg. Med. Chem. 27 (2019) 2427-2437.
[28] N.T. Chandrika, S.K. Shrestha, H.X. Ngo, S. Garneau-Tsodikova, Synthesis and investigation of novel benzimidazole derivatives as antifungal agents, Bioorg. Med. Chem. 24 (2016), 3680-3686.
[29] Y. Dong, M. Liu, J. Wang, Z. Ding, B. Sun, Construction of antifungal dual- target (SE, CYP51) pharmacophore models and the discovery of novel antifungal inhibitors, RSC Adv. 9 (2019) 26302-26314.
[30] D. Zhao, S. Zhao, L. Zhao, X. Zhang, P. Wei, C. Liu, C. Hao, B. Sun, X. Su, M. Cheng, Discovery of biphenyl imidazole derivatives as potent antifungal agents: Design, synthesis, and structure-activity relationship studies, Bioorg. Med. Chem. 25 (2017) 750-758.
[31] Y. Antov, A. Barbul, H. Mantsur, R. Korenstein, Electroendocytosis: exposure of cells to pulsed low electric fields enhances adsorption and uptake of macr omolecules, Biophys J. 88 (2005) 2206-2223.
[32] L. Yuan, M. Liu, G. Liu, D. Li, Z. Wang, B. Wang, J. Han, M. Zhang, Competitive binding of (-)-epigallocatechin-3-gallate and 5-fluorouracil to human serum albumin: A fluorescence and circular dichroism study, Spectrochim, Acta. A. Mol. Biomol. Spectrosc. 173 (2017) 584-592.
[33] B.Sun, H. Zhang, Y. Dong, L. Zhao, J. Han, M. Liu, Evaluation of the combination mode and features of p38 MAPK inhibitors: construction of different pharmacophore models and molecular docking, Mol Simulat. 45(2019) 975-984.
[34]L. Zhao, N. Sun, L. Tian, S. Zhao , B. Sun, Y. Sun, D. Zhao, Strategies for the development of highly selective cytochrome P450 inhibitors: Several CYP targets in current research, Bioorg Med Chem Lett. 29(2019) 2016-2024.

Graphical Abstract

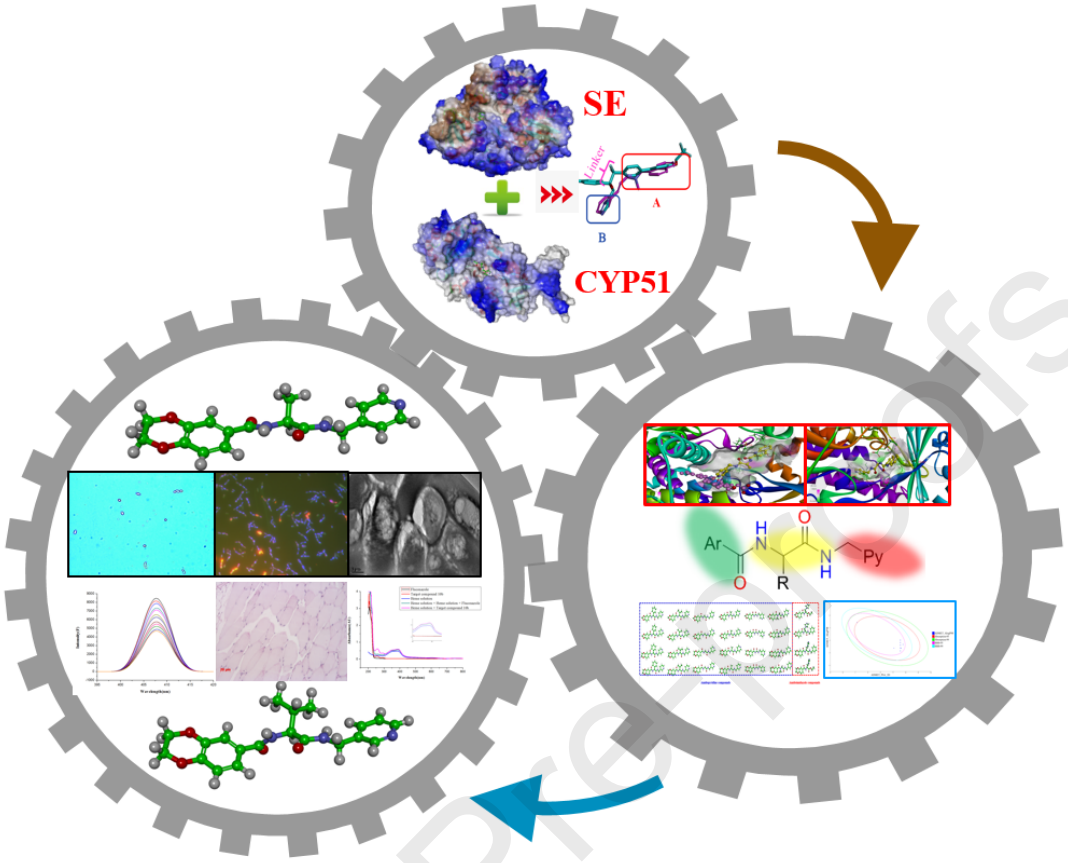

Highlights

1. 28 new compounds with arylamide scaffolds were designed and synthesized as novel dual-target antifungal inhibitors.
2. Compounds **10b** and **11c** were identified as the potent and lead molecules.
3. Compounds **11b** exhibits excellent inhibitory activity against drug-resistant pathogenic fungi.
4. Preliminary mechanism studies of compounds were proved.
5. The target compounds **10b** and **11c** show excellent drug-forming properties

Declaration of interests

☒ The authors declare that they have no known competing financial interests or personal relationships that could have appeared to influence the work reported in this paper.